(article starts on next page)

The XXL Survey: second series

The XXL Survey

XXXIV. Double Irony in XXL-North: a tale of two radio galaxies in a supercluster at *z* = 0.14[⋆]

C. Horellou[1], H. T. Intema[2], V. Smolčić[3], A. Nilsson[1], F. Karlsson[1], C. Krook[1], L. Tolliner[1], C. Adami[4],
C. Benoist[5], M. Birkinshaw[6], C. Caretta[7], L. Chiappetti[8], J. Delhaize[3], C. Ferrari[5], S. Fotopoulou[9],
V. Guglielmo[10,16], K. Kolokythas[11], F. Pacaud[12], M. Pierre[13], B. M. Poggianti[10], M. E. Ramos-Ceja[12],
S. Raychaudhury[11], H. J. A. Röttgering[2] and C. Vignali[14,15]

[1] Chalmers University of Technology, Department of Space, Earth and Environment, Onsala Space Observatory, 439 92 Onsala,
  Sweden
  e-mail: `cathy.horellou@chalmers.se`
[2] Leiden Observatory, Leiden University, Niels Bohrweg 2, 2333 CA, Leiden, The Netherlands
[3] Department of Physics, Faculty of Science, University of Zagreb, Bijenička cesta 32, 10000 Zagreb, Croatia
[4] Aix Marseille Univ., CNRS, CNES, LAM, Marseille, France
[5] Laboratoire Lagrange, Université Côte d'Azur, Observatoire de la Côte d'Azur, CNRS, Bd de l'Observatoire, CS 34229,
  06304 Nice Cedex 4, France
[6] H.H. Wills Physics Laboratory, University of Bristol, Tyndall Avenue, Bristol BS8 1TL, UK
[7] Departamento de Astronomía, DCNE-CGT, Universidad de Guanajuato; Callejón de Jalisco, s/n, Col. Valenciana, 36240,
  Guanajuato, Gto., Mexico
[8] INAF, IASF Milano, via Bassini 15, 20133 Milano, Italy
[9] Centre for Extragalactic Astronomy, Department of Physics, Durham University, South Road, Durham DH1 3LE, UK
[10] INAF – Astronomical Observatory of Padova, 35122 Padova, Italy
[11] Inter-University Centre for Astronomy and Astrophysics, Pune 411007, India
[12] Argelander-Institut für Astronomie, Universität Bonn, Auf dem Hügel 71, 53121 Bonn, Germany
[13] AIM, CEA, CNRS, Université Paris-Saclay, Université Paris Diderot, Sorbonne Paris Cité, 91191 Gif-sur-Yvette, France
[14] Dipartimento di Fisica e Astronomia, Alma Mater Studiorum, Università degli Studi di Bologna,Via Gobetti 93/2, 40129 Bologna,
  Italy
[15] INAF – Osservatorio di Astrofisica e Scienza dello Spazio,Via Gobetti 93/3, 40129 Bologna, Italy
[16] Max-Planck-Institut für Extraterrestrische Physik, Giessenbachstrasse 1, 85748 Garching bei München, Germany

ABSTRACT

*Aims.* We show how the XXL multiwavelength survey can be used to shed light on radio galaxies and their environment.
Methods. Two prominent radio galaxies were identified in a visual examination of the mosaic of XXL-North obtained with the
Giant Metrewave Radio Telescope at 610 MHz. Counterparts were searched for in other bands. Spectroscopic redshifts from the
GAMA database were used to identify clusters and/or groups of galaxies, estimate their masses with the caustic method, and quantify
anisotropies in the surrounding galaxy distribution via a Fourier analysis.
Results. Both radio galaxies are of FR I type and are hosted by early-type galaxies at a redshift of 0.138. The first radio source, named
the Exemplar, has a physical extent of ~400 kpc; it is located in the cluster XLSSC 112, which has a temperature of ~2 keV, a total mass
of ~10^{14} $M_\odot$, and resides in an XXL supercluster with eight known members. The second source, named the Double Irony, is a giant
radio galaxy with a total length of about 1.1 Mpc. Its core coincides with a cataloged point-like X-ray source, but no extended X-ray
emission from a surrounding galaxy cluster was detected. However, from the optical data we determined that the host is the brightest
galaxy in a group that is younger, less virialized, and less massive than the Exemplar's cluster. A friends-of-friends analysis showed
that the Double Irony's group is a member of the same supercluster as the Exemplar. There are indications that the jets and plumes of
the Double Irony have been deflected by gas associated with the surrounding galaxy distribution. Another overdensity of galaxies (the
tenth) containing a radio galaxy was found to be associated with the supercluster.
Conclusions. Radio Galaxies can be used to find galaxy clusters/groups that are below the current sensitivity of X-ray surveys.

Key words. radiation mechanisms: non-thermal – radio continuum: galaxies – galaxies: active – galaxies: magnetic fields –
methods: data analysis

[⋆] FITS files of the GMRT 610 MHz radio images of the two radio galaxies are only available at the CDS via anonymous ftp to
`cdsarc.u-strasbg.fr` (`130.79.128.5`) or via `http://cdsarc.u-strasbg.fr/viz-bin/qcat?J/A+A/620/A19`
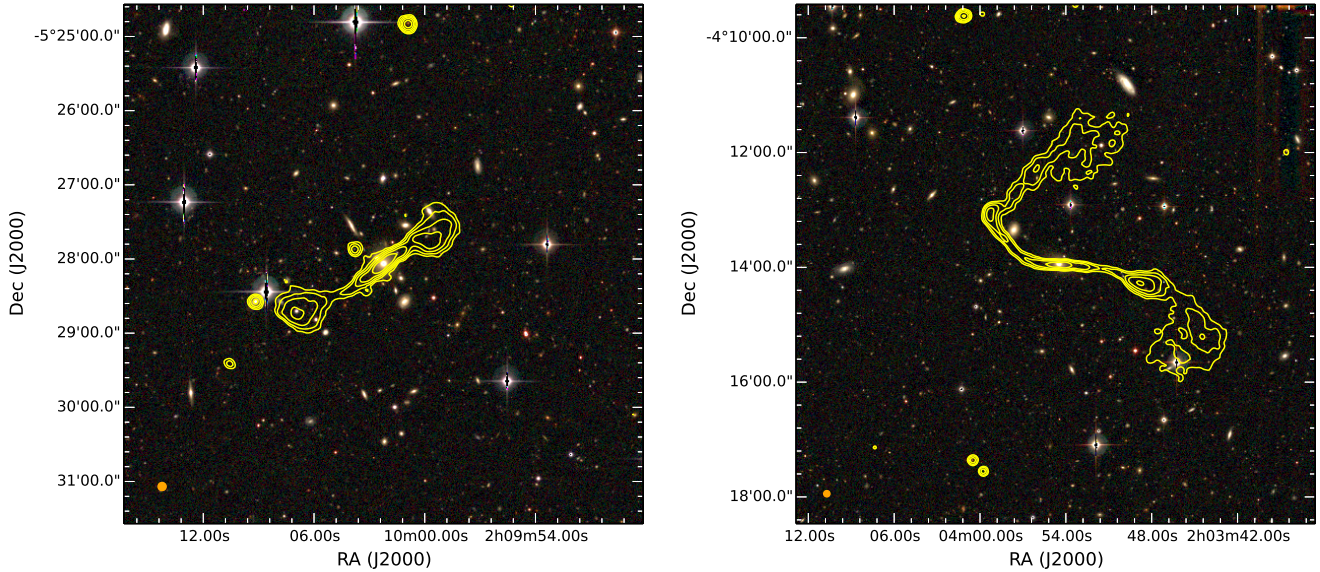
Fig. 1. *Left panel*: Exemplar. The size of the image is $7' \times 7'$. *Right panel*: Double Irony. The size of the image is $9' \times 9'$. Both images show GMRT 610 MHz isocontours superimposed on three-color (*gri*) CFHT images of the fields. The contour levels increase by a factor of two from 0.3 mJy beam^{-1} (which corresponds to 5σ) to 4.8 mJy beam^{-1}. The synthesized beam (6$\farcs$5) is shown in orange in the bottom left corner of each image.

1. Introduction

The study of radio galaxies benefits enormously from a multiwavelength approach, from the X-ray to the radio (e.g., Worrall & Birkinshaw 2006). X-ray emission can be produced both by the active galactic nucleus (AGN) and the diffuse surrounding hot gas. Optical and infrared imaging and spectroscopy provide valuable information on the host galaxy, which most of the time is an early-type galaxy with very little or no star formation (some host galaxies, however, do contain dust and gas in a disk; e.g., Duah Asabere et al. 2016). In the radio, synchrotron radiation directly shows the extent and structure of the emitting plasma that contains relativistic electrons and magnetic fields. The jets may cover tens to hundreds of kiloparsecs before terminating in extended lobes. These jets and lobes may heat the intergalactic gas, displace material, and create cavities and shocks that are seen in the X-ray surface brightness distribution of galaxy clusters (e.g., McNamara et al. 2005). This process, called radio-mode AGN feedback, is believed to play an important role in preventing gas infall on the host galaxy and regulating its evolution (e.g., Croton et al. 2006).

The XXL survey (Pierre et al. 2016, hereafter XXL Paper I) is particularly well suited to the study of AGN and galaxy clusters. With a total observing time of 6.9 Ms, it is the largest X-ray survey carried out by *XMM-Newton*. It covers two fields of 25 square degrees each, one in the southern hemisphere (XXL-South) and the other at an equatorial declination (XXL-North). The X-ray observations have been complemented by an extensive multiwavelength program[1].

In this paper we discuss two double-lobed radio galaxies (see Fig. 1) that we have identified in the mosaic of XXL-North obtained with the Giant Metrewave Radio Telescope (GMRT). The GMRT-XXL-N 610 MHz survey is presented in this issue (Smolcic et al. 2018, hereafter XXL Paper XXIX). It is of interest to compare the properties of the two sources as they are both at the same redshift ($z \simeq 0.14$) and the exact same data set is available for both. Their redshift is near the peak of the redshift

distribution of the most securely detected clusters in XXL (Giles et al. 2016, hereafter XXL Paper III). As our analysis shows, the radio galaxies are both part of the same supercluster, but their immediate surroundings are different.

The first radio galaxy appears regular, with symmetric jets leading to two radio lobes. It is located at the center of a cluster and hosted by the brightest cluster galaxy (BCG), both of which have been detected and characterized in studies of the sample of the brightest 100 XXL clusters (Pacaud et al. 2016, hereafter XXL Paper II; XXL Paper III; Lieu et al. 2016, hereafter XXL Paper IV; Eckert et al. 2016, hereafter XXL Paper XIII; Lavoie et al. 2016, hereafter XXL Paper XV). Because of its appearance with twin jets and plumes and its association with an early-type galaxy in a cluster, we refer to this source in the remainder of this paper as *the Exemplar*. The other radio galaxy stands out for its very large extent (a total length of $7\farcm56$, or 1100 kpc in our adopted cosmology[2]) and its peculiar shape reminiscent of two reversed question marks, the reason why we named it *the Double Irony*[3].

This paper is organized as follows. The available data sets are presented in Sect. 2. In Sect. 3 we discuss the Exemplar radio galaxy, its host galaxy, and host cluster; the radio images are presented and analyzed. Section 4 is about the Double Irony and follows a similar structure; an overdensity of galaxies is found. In Sect. 5 the two radio galaxies are compared and discussed. In particular, the distributions of surrounding galaxies are examined in relation to the orientation of the radio galaxies to search for environmental effects. In Sect. 6 it is shown that the group of galaxies associated with the Double Irony radio galaxy is part of the same supercluster as the Exemplar's cluster and this large-scale structure is discussed. In Sect. 7 we discuss the

---

[1] http://xxlmultiwave.pbworks.com

[2] Throughout this paper and for consistency with the first XXL series of papers, we use the WMAP9 cosmology ($\Omega_{\rm m} = 0.28$, $\Omega_{\Lambda} = 0.72$, $H_0 = 70$ km s^{-1} Mpc^{-1}; Hinshaw et al. 2013). At the redshift of the radio galaxies discussed here ($z \simeq 0.138$), this gives a scale of 2.443 kpc/arcsec and a luminosity distance of 652.5 Mpc.

[3] The percontation point (a reversed question mark, ⸮) was invented by the English printer Henry Denham at the end of the sixteenth century to mark the end of a rhetorical question and was later used to denote Irony.

Table 1. Characteristics of the radio images.

Survey	Frequency (MHz)	Resolution ('')	Pixel size ('')	σ (mJy beam^{-1})
TGSS ADR1	150	25	6.4	5.0
GMRT-XXL-N	610	6.5	1.9	0.060
FIRST	1400	6.8×5.4	1.8	0.15
NVSS	1400	45	15	0.45 (I), 0.29 (Q, U)

occurrence of radio galaxies in superclusters and their potential use as tracers of the large-scale structure. We conclude in Sect. 8.

2. Data and data analysis

2.1. Radio

As detailed below, we used images at three different frequencies obtained from four different surveys carried out with the Very Large Array (VLA) and the GMRT. These surveys have different sensitivities and angular resolutions, and are also sensitive to different angular scales. The characteristics of the data are summarized in Table 1.

The most important data set is the GMRT-XXL-N 610 MHz radio continuum survey described in XXL Paper XXIX. XXL-North contains the XMM-LSS area that was observed earlier with the GMRT (Tasse et al. 2006, 2007). The rest of the XXL-North field was recently observed at higher sensitivity, and the data were combined. The final mosaic has an angular resolution of 6.''5. The two radio galaxies discussed here are located outside the XMM-LSS region, in the newly covered region of 12.66 square degrees that has an average sensitivity of 45 μJy beam^{-1}.

The other radio continuum data were taken from the following, publicly available surveys:

– the Tata Institute of Fundamental Research (TIFR) GMRT Sky Survey (TGSS) first alternative data release (TGSS ADR1) at 150 MHz and 25'' resolution (Intema et al. 2017);
– the Faint Images of the Radio Sky at Twenty Centimeters (FIRST) at 1.4 GHz, 6.''8 × 5.''4 resolution (Becker et al. 1995; Helfand et al. 2015);
– the NRAO VLA Sky Survey (NVSS) at 1.4 GHz, 45'' resolution (Condon et al. 1998). NVSS also contains polarization information. We downloaded Stokes Q and U images from the NVSS website[4] and produced images of the polarized intensity and of the polarization angle using the task POLC in the Astronomical Image Processing System[5] (AIPS) that corrects for the Ricean bias in polarized intensity (Wardle & Kronberg 1974).

Total-intensity images do not always do justice to the details of the surface brightness distributions in astronomical sources. Images of the norm of the intensity gradient, $|\nabla I|$, have been used to reveal the paths of jets and substructures in radio galaxies (e.g., Laing et al. 2011). We computed images of $|\nabla I|$ at 610 MHz using a Sobel filter (Sobel & Feldman 1968, unpublished, reported in Wikipedia[6]).

Flux densities and spectral indices were measured within defined regions. The statistical uncertainties on the flux density measurements were calculated as $\sigma \sqrt{N_{\text{beam}}}$, where σ is the

standard deviation of the noise and N_{beam} is the number of beams within the region.

The survey images were used and no attempt was made to re-image the data to match the (u, v) ranges or the imaging weighting scheme. Only the FIRST image of the Double Irony may have extended emission that has been filtered out (the largest angular scale of FIRST is 2'), and this is discussed in Sect. 4.3.2. The sources are barely resolved in TGSS and in NVSS, and some of the features of the Double Irony are only marginally detected in TGSS, leading to large uncertainties in the flux measurements that would not be improved much by re-imaging.

Throughout the paper we use the following convention for the radio spectral index, α: $S_\nu \propto \nu^\alpha$, where S_ν is the flux density at frequency ν. The uncertainties on the spectral indices measured between two frequencies were calculated using standard error propagation,

$$\Delta\alpha = \sqrt{\left(\frac{\Delta S_1}{S_1}\right)^2 + \left(\frac{\Delta S_2}{S_2}\right)^2} \bigg/ \ln\left(\frac{\nu_2}{\nu_1}\right), \tag{1}$$

where ΔS_i is the uncertainty on the flux density S_i measured at frequency ν_i and $\nu_2 > \nu_1$.

A systematic uncertainty of 10% on each flux density measurement (due to uncertainties on the absolute flux calibration and from the imaging process) results in the following systematic uncertainties on the spectral indices (Eq. (1)):

$$\Delta\alpha_{\text{sys}}(\nu_1, \nu_2) = \begin{cases} 0.10 \\ 0.17 \\ 0.06 \end{cases} \text{ if } \frac{\nu_1}{\nu_2} = \begin{cases} 150 \text{ MHz}/610 \text{ MHz} \\ 610 \text{ MHz}/1400 \text{ MHz} \\ 150 \text{ MHz}/1400 \text{ MHz} \end{cases}. \tag{2}$$

2.2. Multiwavelength

We used data from the following surveys.

– The X-ray measurements with *XMM-Newton* and the XXL project are described in XXL Paper I. The cluster catalogs are presented in XXL Paper II and XXL Paper XX, and the AGN catalogs by Fotopoulou et al. (2016, XXL Paper VI) and by Chiappetti et al. (2018, hereafter XXL Paper XXVII).
– There is a large overlap between XXL-North and the CFHT-LS W1 region covered in several optical bands by the Canada-France-Hawaii Telescope (CFHT). All XXL-North clusters but five have *ugriz* photometry from MegaCam (Gwyn 2012).
– The Sloan Digital Sky Survey (SDSS) Data Release 14 (SDSS DR14[7]) contains optical and near-infrared images of our fields and spectra of some of the sources.
– The Galaxy and Mass Assembly (GAMA) database[8] contains spectra, spectroscopic redshifts, and information on the detected spectral lines for the host galaxies of our two radio sources and other galaxies in the field (Baldry et al. 2018).

---

[4] http://www.cv.nrao.edu/nvss
[5] http://www.aips.nrao.edu
[6] https://en.wikipedia.org/wiki/Sobel_operator, page last edited on 22 February 2018, at 14:58.

[7] http://skyserver.sdss.org/dr14
[8] http://www.gama-survey.org

Table 2. Characteristics of the cluster of galaxies XLSSC 112 and of the BCG hosting the Exemplar radio galaxy.

| Quantity	Value	Notes
Cluster name	XLSSC 112	(1)
$RA_{cluster}(J2000)$	$32°514$	(1)
$Dec_{cluster}(J2000)$	$-5°462$	(1)
$z_{cluster}$	0.139	(1)
$N_{galaxies}$	14	(1)
$L_{500,MT}^{XXL}$	$(0.61 \pm 0.08) \cdot 10^{43}$ erg s^{-1}	(1)
F_{60}	$(5.89 \pm 0.62) \cdot 10^{-17}$ Wm^{-2}	(2)
$T_{300\,kpc}$	$1.76^{+0.25}_{-0.15}$ keV	(2)
$M_{500,MT}$	$(9.0 \pm 4.1) \cdot 10^{13}\,M_\odot$	(2)
$r_{500,MT}$	0.653 Mpc	(2)
$M_{gas,500}$	$(0.42 \pm 0.12) \cdot 10^{13}\,M_\odot$	(3)
$r_{500,WL}$	$0.6^{+0.1}_{-0.2}$ Mpc	(4)
$M_{500,WL}$	$0.8^{+0.6}_{-0.5} \cdot 10^{14}\,M_\odot$	(4)
$M_{200,WL}$	$1.2^{+0.9}_{-0.8} \cdot 10^{14}\,M_\odot$	(4)
RA_{BCG} (J2000)	$32°5093$	(5)
Dec_{BCG} (J2000)	$-5°4678$	(5)
Offset from X-ray center	$24''5$	(5)
z_{BCG}	0.138	(5)
M_{BCG}	$5.35^{+0.41}_{-0.29} \cdot 10^{11}\,M_\odot$	(5)
$M_{stellar}$	$2.13^{+0.30}_{-0.56} \cdot 10^{11}\,M_\odot$	(6)
SFR1 (2–20 Myr ago)	$0\,M_\odot$ yr^{-1}	(6)
SFR2 (20–600 Myr ago)	$5.6\,M_\odot$ yr^{-1}	(6)
SFR3 (0.6–5.6 Gyr ago)	$46.2\,M_\odot$ yr^{-1}	(6)
SFR4 (> 5.6 Gyr ago)	$14.9\,M_\odot$ yr^{-1}	(6)
LW-age	3.6×10^9 yr	(6)
MW-age	5.8×10^9 yr	(6)
σ_V	282.0 ± 8.6 km s^{-1}	(7)
$z_{SDSS\,DR14}$	0.13818 ± 0.00002	(7)
z_{GAMA}	0.13814	(8)

Notes. The first three blocks give cluster properties, while the others refer to the BCG. (1) X-ray and optical characteristics from XXL Paper II. $N_{galaxies}$ is the number of galaxies on which the mean redshift, $z_{cluster}$, was based. (2) X-ray-derived quantities from XXL Paper III. F_{60} is the [0.5–2] keV flux within a 1′ radius; $T_{300\,kpc}$ is the temperature within 300 kpc; the other quantities are the total mass and gas mass within a radius of r_{500}. (3) Gas mass within r_{500} from XXL Paper XIII. (4) Weak lensing mass and size estimates from XXL Paper IV. (5) Characteristics of the BCG from XXL Paper XV. M_{BCG} refers to the stellar mass of the BCG. (6) This work. $M_{stellar}$ is the stellar mass of the BCG estimated from spectral model-fitting. SFR refers to the star formation rate in four different periods, derived from model-fitting the GAMA spectrum. LW and MW refer to the luminosity-weighted and the mass-weighted age. (7) Velocity dispersion of the galaxy, from the Baryon Oscillation Spectroscopic Survey (BOSS; SDSS DR14, SDSS 021002.24-052804.1) and spectroscopic redshift. (8) Spectroscopic redshift from GAMA (GAMA J021002.23-052804.1).

– The Wide-field Infrared Survey Explorer (WISE; Wright et al. 2010) has detected the host galaxies of our two radio sources in several bands.

3. The Exemplar

In Fig. 2 we show a multiband false-color image of the field of the Exemplar: the optical image is shown in green, the X-ray emission in blue and in contours, and the 610 MHz radio
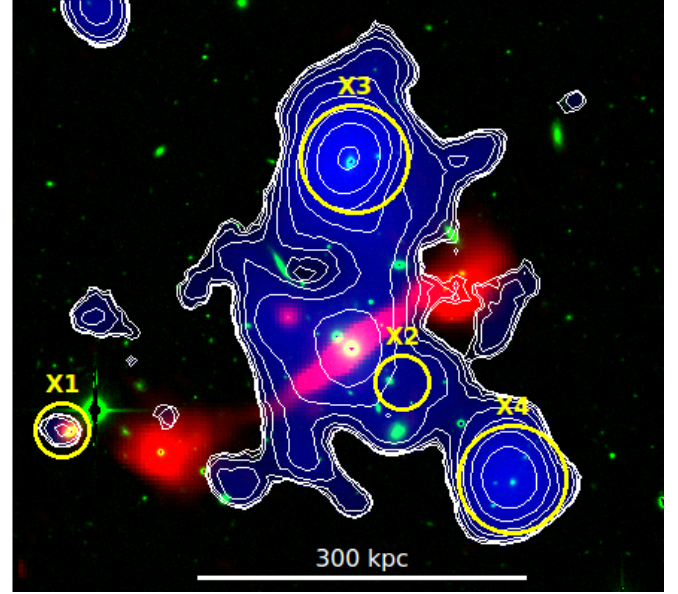
Fig. 2. Multiband false-color image of the Exemplar: X-ray emission in the [0.5–2] keV band in blue, optical emission (*i*-band CFHT image) in green, radio emission (GMRT 610 MHz) in red. The ten contours showing the X-ray surface brightness increase logarithmically between 3×10^{-17} and 6×10^{-16} erg s^{-1} cm^{-2}. Four X-ray point sources are visible in the image, labeled X1 to X4 above the yellow circles that indicate their positions. The point sources were subtracted before calculating the flux density of the cluster given in XXL Paper II and quoted in Table 2, but they are shown in this image. X3 corresponds to 3XLSS J021002.1-052655 and X4 to 3XLSS J020958.2-052853 in the XXL point source catalog (XXL Paper XXVII). There are optical counterparts to X3 (a galaxy at photometric redshift of 0.028 ± 0.014, SDSS J021002.25-052655.5) and to X4 (a galaxy at a photometric redshift of 0.351 ± 0.118, SDSS J020958.27-052853.5). The other two X-ray sources did not match the criteria to be included in the X-ray catalog. The size of the image is about $4' \times 4'$. Diffuse X-ray emission is seen, and is associated with the galaxy cluster XLSSC 112.

emission from the GMRT in red. Several X-ray point sources are seen, in addition to diffuse X-ray emission associated with a cluster. The two brightest X-ray point-like sources (X3 and X4) are galaxies with optical counterparts and photometric redshifts in SDSS DR14; they are not associated with the cluster (see caption of Fig. 2). The fainter X-ray source X1 coincides with the radio source S1 (see discussion in Sect. 3.2). It has an optical galaxy counterpart, but no redshift is available.

3.1. Host galaxy in the cluster XLSSC 112 in the supercluster XLSSsC N03

In Table 2 we list some characteristics of the cluster of galaxies XLSSC 112 and of the BCG hosting the Exemplar radio galaxy.

3.1.1. Cluster XLSSC 112

The Exemplar is located at the center of a galaxy cluster listed among the 100 brightest clusters in XXL (XXL Paper II). Cataloged as XLSSC 112 the cluster has a mean redshift of $z = 0.139$ calculated from the spectroscopic redshifts of 14 member galaxies (Table 2). The intracluster gas has a temperature of ~1.8 keV measured within the central radius of 300 kpc (XXL Paper III). The total cluster mass was estimated from a mass–temperature scaling relation (XXL Paper III) and from weak gravitational lensing (XXL Paper IV), yielding consistent values of about

Table 3. Flux density measurements in the different regions of the Exemplar shown in Fig. 3.

Region	$S_{150\,\text{MHz}}$ (mJy)	$S_{610\,\text{MHz}}$ (mJy)	$S_{1.4\,\text{GHz}}$ (FIRST) (mJy)	$S_{1.4\,\text{GHz}}$ (NVSS) (mJy)
S1	25.73 ± 3.11	3.27 ± 0.14	0.97 ± 0.40	–
S2	6.74 ± 3.30	2.48 ± 0.14	1.38 ± 0.40	–
A (SE lobe)	61.14 ± 9.46	32.25 ± 0.43	8.21 ± 1.19	12.98 ± 0.37
B (NW lobe)	71.98 ± 7.85	38.76 ± 0.36	13.11 ± 1.00	10.91 ± 0.28
C	97.07 ± 10.94	56.64 ± 0.50	29.89 ± 1.40	30.60 ± 0.41
C \ S2	90.33 ± 11.42	54.16 ± 0.52	28.52 ± 1.45	29.23 ± 0.44
T	284.79 ± 26.63	138.16 ± 1.21	44.81 ± 3.38	74.95 ± 0.99
$T_{A \cup B \cup C}$	230.20 ± 16.45	127.66 ± 0.75	51.21 ± 2.09	54.50 ± 0.63
$T_{(A \cup B \cup C) \setminus (S1 \cup S2)}$	197.72 ± 28.60	121.90 ± 1.30	48.87 ± 3.63	52.16 ± 1.09
$T \setminus (S1 \cup S2)$	252.32 ± 27.01	132.40 ± 1.23	42.47 ± 3.43	72.61 ± 1.01

Notes. The coordinates of S1 and S2 are given in the caption of Fig. 3. The flux densities of S1 and S2 at 150 MHz were extrapolated from the measurements at 610 and 1400 MHz (FIRST). The symbols $\cup$ and $\setminus$ are taken from set theory and are used to indicate a union and an exclusion, respectively: for instance, C $\setminus$ S2 means that the flux density from source S2 was subtracted from that measured in the central (C) region; $T_{A \cup B \cup C}$ is the flux density measured by summing the measurements in the regions A (SE lobe), B (NW lobe), and C (central region). The 1.4 GHz flux densities of S1 and S2, which are point-like, were taken from FIRST.

$10^{14}\,M_\odot$ within a radius $r_{500} = 0.6$ Mpc (the parameter r_{500} is the radius within which the mean density is 500 times the critical density of the universe at the cluster's redshift).

3.1.2. Supercluster XLSSsC N03

The cluster was found to be part of a larger structure of seven clusters, all at a redshift of $z \simeq 0.14$, with a total mass of about $10^{15}\,M_\odot$ (XLSSC-b; XXL Paper II). Five such super-structures were identified in the sample of the 100 brightest clusters in XXL using a friends-of-friends algorithm in 3D space (XXL Paper II). New supercluster candidates were found in the larger sample of 365 clusters cataloged by Adami & et al. (2018, hereafter XXL Paper XX). The five superclusters identified in XXL Paper II were confirmed. However, the supercluster hosting the Exemplar, which was described as a double structure in XXL Paper II, with an eastern component of four clusters and a western component of three clusters (including XLSSC 112), has been split into two superclusters in the new study: the four clusters in the eastern part form XLSSsC N08, at a mean redshift of $z = 0.141$, and the three clusters in the western part joined five other clusters to form a larger structure, the supercluster XLSSsC N03, at a mean redshift of $z = 0.139$ (XXL Paper XX). XLSSC 112 is therefore affiliated to a supercluster with eight cluster members. This is discussed in Sect. 6 (see also Fig. 14).

3.1.3. Brightest cluster galaxies and the nearest neighbor

The properties of the BCG of the 100 brightest XXL clusters have been studied in XXL Paper XV. Guglielmo et al. (2018a, XXL Paper XXII) have assembled a catalog of optically detected galaxies in the X-ray-detected clusters and groups of XXL-North. In Fig. A.1 (top panel) we show the GAMA spectrum of the BCG, typical of an old stellar population. We fitted the GAMA spectrum using the full spectral fitting code SINOPSIS (Fritz et al. 2007) and obtained an estimate of its stellar mass of about $2 \times 10^{11}\,M_\odot$ (using a Chabrier 2003 initial mass function). This is lower than had been estimated from broadband photometry (XXL Paper XV). This analysis also provided an estimate of the star formation history of the galaxy. The characteristics of the cluster and of its BCG are summarized in Table 2.

There is a second, smaller galaxy located 7″ to the NE of the BCG (about 17 kpc on the sky) at a similar redshift ($z = 0.13623$,

galaxy GAMA J021002.58-052759.8). Companions like this are very common for radio sources of this type (e.g., 3C 296).

3.2. Radio

3.2.1. Radio morphology

Figure 3 shows the four radio continuum images of the Exemplar used in this work. The Exemplar has two jets and lobes that appear clearly in the higher resolution images (GMRT 610 MHz and the FIRST 1.4 GHz images, Figs. 3b and d), but are not resolved in the lower resolution images (TGSS and NVSS; Figs. 3a and c). The TGSS ADR1 catalog of Intema et al. (2017) lists three individual Gaussian sources[9]. The NVSS catalog lists two sources[10] (Condon et al. 1998). The XXL-GMRT-610 MHz catalog[11] lists three resolved sources within a radius of 4′ from the core of the Exemplar (XXL Paper XXIX). From end to end the radio source stretches over 160″ (396 kpc) in the GMRT 610 MHz image.

Zooming into the central region, we see that the radio surface brightness peaks about 3″5 (8.7 kpc) away from the optical center of the BCG on either side of the jets, with a flux density of about 8.8 mJy in the NW and 9.8 mJy to the SE at 610 MHz. There are two corresponding sources in the FIRST catalog[12]. We note that these brighter radio spots are located just outside the optical extent of the host galaxy. No cataloged

---

[9] TGSS J021006-052841, which corresponds to the SE lobe, is listed as an isolated single-Gaussian source with a flux density of 57.2 ± 7.0 mJy; TGSS J021002-052804, which corresponds to the core and the inner jets, has 90.5 ± 9.9 mJy; TGSS J020959-052738, which corresponds to the NW lobe, has 73.3 ± 3.3 mJy. The second and third sources overlap.
[10] NVSS J021007-052842 has a total flux density of 15.3 ± 1.0 mJy. NVSS J021001-052758 has a total flux density 58.8 ± 2.2 mJy.
[11] The three sources listed as resolved within a radius of 4′ from the core of the Exemplar are XXL-GMRT J021006.7-052840, XXL-GMRT J021004.3-052826, and XXL-GMRT J021000.9-052753. The two compact sources that we named S1 and S2 are XXL-GMRT J021009.1-052834 and XXL-GMRT J021003.7-052751, respectively.
[12] FIRST J021001.9-052800 with a peak flux density of 4.15 mJy beam^{-1} (integrated flux density $S_T = 5.53$ mJy) and FIRST J021002.4-052806 with a peak flux density of 6.32 mJy beam^{-1} ($S_T = 10.19$ mJy). From the peak values this gives a spectral index of -0.90 for the fainter NW peak and -0.53 for the SE peak between 610 MHz and 1.4 GHz.
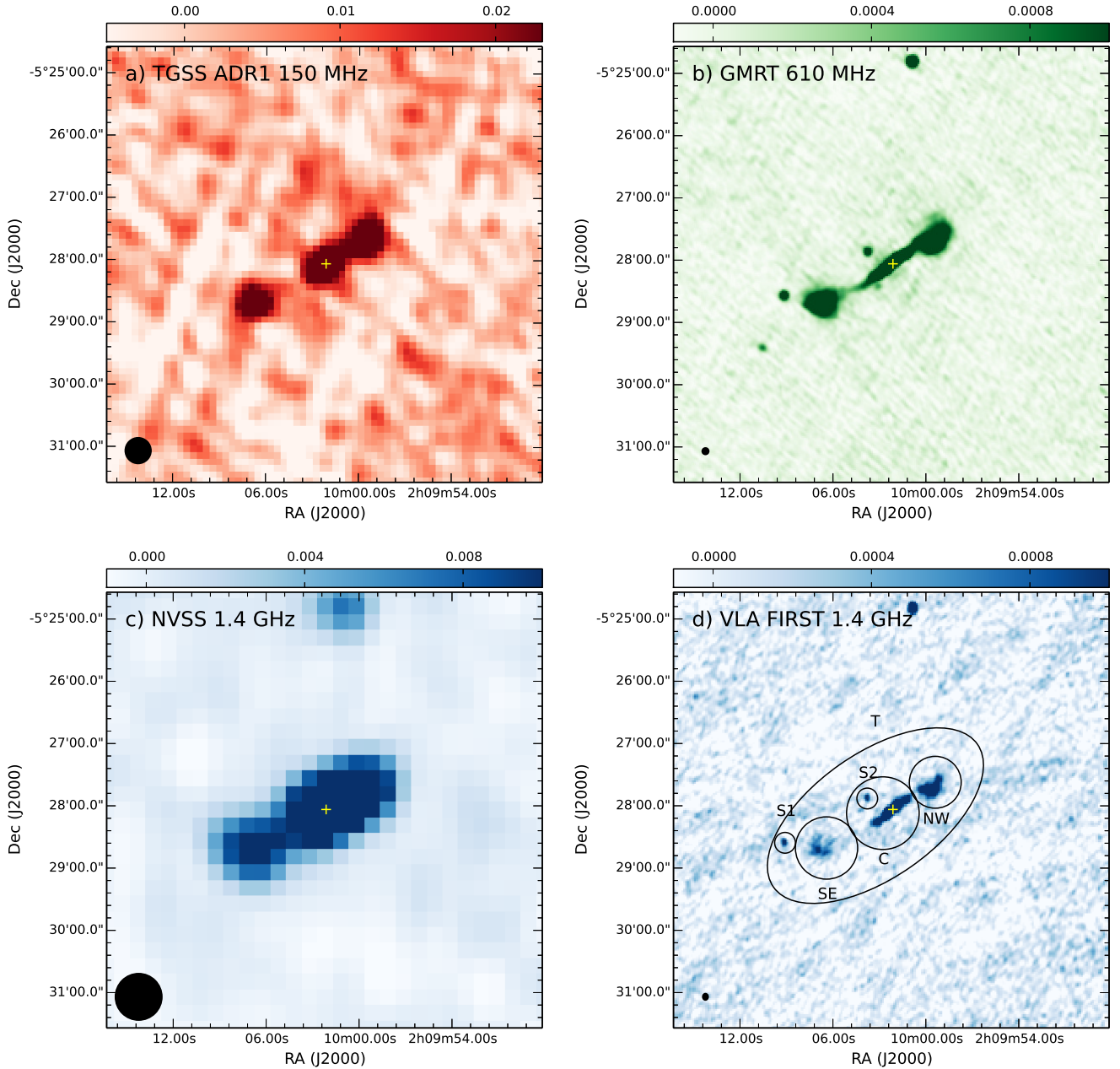
Fig. 3. Radio continuum images of the Exemplar: *a*) from the TGSS ADR1 at 150 MHz; *b*) from the GMRT at 610 MHz; *c*) from the NVSS at 1.4 GHz; *d*) from FIRST at 1.4 GHz. The size of the synthesized beam is indicated in the bottom left corner of each image. The position of the BCG is shown by a yellow cross. The circles and ellipses overlaid on the FIRST 1.4 GHz image show the regions used for the photometry and the spectral index measurements (see Tables 3 and 4). The NW aperture is a circle with a radius of 25″, centered at (32°49747, −5°46036). The aperture in the central region (C) is a circle with a radius of 35″, centered at (32°51157, −5°46863). The SE circular aperture has a radius of 30″, centered at (32°52672, −5°47796). The ellipse (T) has a semimajor axis of 2′, a semiminor axis of 1′, and a position angle of +125° measured counterclockwise from the north, centered at (32°51357, −5°46929). The position of S1 is (32°53811, −5°47619) and that of S2 is (32°51574, −5°46446) and the circles have a radius of 10″.

FIRST source is found at the central location of the BCG. The radio core is unresolved and is likely embedded in the jet and/or is synchrotron self-absorbed.

The jets have position angles of +130° and −50° (measured counterclockwise from the north). They are straight out to a distance of 32″ to the NW and 40″ to the SE from the center of the BCG, at which point they change direction and turn right (that is, the NW jet turns toward the W and the SE jet turns toward the E). The NW jet moves into two brighter regions embedded in a diffuse lobe. The SE jet continues to grow fainter but remains collimated for another 15″ before reaching a

diffuse lobe. This morphology suggests an interaction with the surrounding medium at a distance of about 80 kpc (30″) to the NW and about 90 kpc (35″) to the SE.

Two compact radio sources are seen near the radio galaxy. They are named S1 and S2 in Tables 3 and 4 and their flux densities and their spectral index were estimated between 610 MHz and 1.4 GHz (FIRST image). The spectral indices are used to estimate the flux at 150 MHz. The contributions of those two sources are subtracted from the total flux densities measured within the regions outlined in Fig. 3. The radio photometry of the Exemplar is presented in the coming section.

Table 4. Spectral index measurements in the different regions of the Exemplar shown in Fig. 3.

Region	$\alpha_{150\ \mathrm{MHz}}^{610\ \mathrm{MHz}}$ (1)	$\alpha_{610\ \mathrm{MHz}}^{1400\ \mathrm{MHz}}$ (2)	$\alpha_{150\ \mathrm{MHz}}^{1400\ \mathrm{MHz}}$ (3)
$\Delta\alpha_{\mathrm{sys}}$	0.1	0.17	0.06
A (SE lobe)	-0.46 ± 0.11	-1.65 ± 0.18	-0.69 ± 0.07
B (NW lobe)	-0.44 ± 0.00	-1.30 ± 0.09	-0.84 ± 0.05
C	-0.38 ± 0.08	-0.77 ± 0.06	-0.52 ± 0.05
C \ S2	-0.36 ± 0.09	-0.77 ± 0.04	-0.51 ± 0.06
T	-0.52 ± 0.07	-1.36 ± 0.09	-0.60 ± 0.04
T \ (S1 ∪ S2)	-0.46 ± 0.08	-1.37 ± 0.06	-0.56 ± 0.05

Notes. The spectral indices were calculated from flux density measurements in (1) the TGSS and the GMRT 610 MHz maps; (2) the GMRT 610 MHz and the FIRST 1.4 GHz maps; (3) the TGSS and the NVSS 1.4 GHz maps. The first line gives the systematic uncertainties on α for a 10% systematic uncertainty on each flux density measurement. The other uncertainties listed in the table are statistical. The meanings of the \ and ∪ symbols were given in the notes of Table 3.
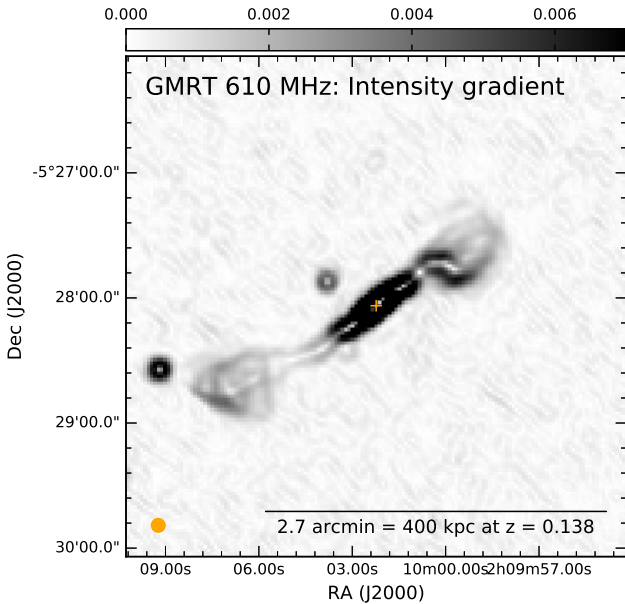
Fig. 4. Grayscale image of the norm of the intensity gradient of the Exemplar at 610 MHz. It reveals the path of the jets and substructures in the brightness distribution of the radio lobes. The beam is shown in orange in the bottom left corner.

In Fig. 4 we show an image of the gradient of the intensity in the GMRT image at 610 MHz, $|\nabla I|$. The path of the jet is clearly delineated in white where the intensity has a local maximum. Strong gradients are seen near the inner jets where the jet bends as it enters the NW lobe, and at the extremity of the SE lobe. Similar features have been seen in deep images of nearby low-luminosity FR I radio galaxies (Laing et al. 2011).

3.2.2. Luminosity, flux density, spectral index

Flux densities were measured at the three different frequencies in the regions indicated in Fig. 3; the values are listed in Table 3.

The spectral luminosity, L_ν, can be calculated following

$$\left(\frac{L_\nu}{\mathrm{W\ Hz^{-1}}}\right) = 5.257 \times 10^{22} \left(\frac{S_\nu}{\mathrm{mJy}}\right)\left(\frac{D_L}{662.8\ \mathrm{Mpc}}\right)^2 . \qquad (3)$$

In the commonly used classification of Fanaroff & Riley (1974), FR I radio galaxies have been observed to have a spectral luminosity lower than 5×10^{25} W Hz^{-1} at 178 MHz, while the FR II radio galaxies are more luminous. The Exemplar has a total flux density of about 250 mJy at 150 MHz (taking an average of the value obtained by summing up the different regions and by measuring in a larger ellipse). For a spectral index of -0.7, this gives $L_{178\ \mathrm{MHz}} \simeq 1.5 \times 10^{25}$ W Hz^{-1}, making it an FR I radio galaxy. Its morphology is also that of an FR I.

Spectral indices were calculated in the regions overlaid on Fig. 3 (Table 4). The central region has flatter spectral indices than the lobes. The spectral indices calculated at high frequencies are systematically steeper than those at low frequencies[13] Using the NVSS 1.4 GHz image and the TGSS 150 MHz image gives intermediate values.

Unfortunately, the quality of the data does not allow a quantitative analysis of the evolution of the cosmic-ray electrons, and deeper images with matching angular resolutions are required to measure the curvature of the radio spectrum.

3.2.3. Polarization

No polarization is seen in the NVSS images of the Exemplar. The lobes have a flux density at 1.4 GHz ranging between 8 and 13 mJy, and the flux density of the core/central region is about 30 mJy (Table 3). The noise level in polarized intensity is about 0.4 mJy in NVSS. So we place a 3σ upper limit on the fractional polarization of 15% in the lobes and 4% in the central region.

4. The Double Irony as a giant radio galaxy

The Double Irony stands out in XXL-North because of its large angular size and peculiar shape. As we show in Sect. 4.3.1, it has a total physical length of about 1.1 Mpc, which makes it a member of the rare class of giant radio galaxies (GRGs), i.e., Mpc-sized radio galaxies. Samples of GRGs have been built based on searches in large radio surveys at GHz frequencies such as the Westerbork Northern Sky Survey[14] (e.g., Schoenmakers et al. 2001); the NVSS[15] and the FIRST survey[16] (e.g., Lara et al. 2001a,b; Machalski et al. 2001; Santiago-Bautista et al. 2016; Proctor 2016), or the Sydney University Molonglo Sky Survey[17] (e.g., Saripalli et al. 2005).

The total number of known GRGs is about 300 (Dabhade et al. 2017), but this number is likely to increase rapidly with the advent of radio surveys at lower frequencies where the flux densities are stronger because most of the emission comes from the more numerous lower energy relativistic electrons that have a longer lifetime. Surveys carried out for example with the LOw Frequency ARray (LOFAR; van Haarlem et al. 2013),

---

[13] Flux loss in the FIRST 1.4 GHz image would produce a similar effect. The largest angular scale to which the FIRST observations are sensitive is 2′ and the radio galaxy stretches over ∼2.′5. On the other hand, the lobes themselves are smaller than 1′ across. For the SE lobe, the flux density measured in the FIRST image within the elliptical region displayed in Fig. 3 is lower than that measured in the NVSS image (about 8.2 vs. 13 mJy, see Table 3), an indication that some of the extended emission might have been filtered out. For the NW lobe on the other hand, the FIRST flux is higher than the NVSS flux, perhaps because the region (within a circle of 50″ diameter) does not include all the flux of the 45″ resolution NVSS image.

[14] WENSS, Rengelink et al. (1997).

[15] NVSS, Condon et al. (1998).

[16] FIRST, Becker et al. (1995), Helfand et al. (2015).

[17] SUMSS, Bock et al. (1999).

MSSS[18] *Herschel*-ATLAS, and LoTSS[19] have begun to reveal even larger GRGs than those discovered at higher frequencies (e.g., Hardcastle et al. 2016; Clarke et al. 2017).

GRGs are interesting in their own right, but also as probes of their environment. As radio lobes expand beyond the halos of their host galaxies, they may interact with the so-called Warm-Hot Intergalactic Medium (WHIM), a diffuse plasma at a temperature of 10^5 to 10^7 K that is associated with galaxies in the large-scale structure (e.g., Subrahmanyan et al. 2008; Safouris et al. 2009). They are therefore, useful probes of the intergalactic medium and possibly even of its evolution if they can be found at high redshift (Machalski et al. 2007). The large sizes of GRGs do not seem to be due to stronger nuclear activity (Ishwara-Chandra & Saikia 1999) and GRGs do not seem to form a class that is fundamentally different from normal-sized radio galaxies (Machalski & Jamrozy 2006; Kuźmicz & Jamrozy 2012). The general picture is that GRGs are able to grow to larger sizes because of their lower density environments and/or simply because they are older (e.g., Jamrozy et al. 2008).

In this section we begin by examining the host galaxy of the Double Irony; then we look at the X-ray information and the galaxy distribution in the optical before presenting the radio maps; finally the possible nature of this unusual radio galaxy is discussed. In the next section the two radio galaxies will be compared and more quantities will be derived.

4.1. Host galaxy

We identify a galaxy with a spectroscopic redshift of $z = 0.13751$ (GAMA J020354.47-041356.8) as the host galaxy of the Double Irony based on its position with respect to the radio contours. The GAMA spectrum is displayed in Fig. A.1 (bottom panel). It is very similar to the spectrum of the host galaxy of the Exemplar, and reflects an old stellar population. We derived an estimate of its stellar mass of about 3×10^{11} $M_\odot$. This analysis provides some insight into the star formation history of the galaxy: it has no ongoing star formation, but had a star formation rate (SFR) of about 1.5 $M_\odot$ yr^{-1} $\sim$ 20–600 Myr ago, and an even higher SFR of $\sim$30–45 $M_\odot$ yr^{-1} in the more distant past (see Table 5).

There is also an X-ray point-like counterpart to the optical/near-IR host (see Table 5). The source is detected only in the [0.5–2] keV band, and the detection is not of sufficient quality to say anything about the nature of the X-ray spectrum (thermal or non-thermal). The corresponding X-ray luminosity is 1.26×10^{41} erg s^{-1}. Ranalli et al. (2003) found a relation between the X-ray luminosity and the SFR of nearby star-forming galaxies. Using their relation (their Eq. 14) gives a SFR estimate of about 28 $M_\odot$ yr^{-1}, which is significantly higher than that inferred from the analysis of the optical spectrum. It is very unlikely that the X-ray emission is related to star formation; since the X-ray emission is point-like and the optical major axis of the galaxy is about 20″ (more than double the full width at half maximum (FWHM) of the point response function of *XMM-Newton*), it indicates that the X-ray emission does not come from hot gas surrounding the elliptical galaxy. We conclude that it is likely to come from the AGN. The signal is, however, very weak, with only about 12 counts, and a detection likelihood of 15.6, just

Table 5. Characteristics of the galaxy hosting the Double Irony radio galaxy.

Quantity	Value	Notes
RA$_{galaxy}$(J2000)	30°97696	(1)
Dec$_{galaxy}$(2000)	−4°23247	(1)
z_{spec}	0.13751	(1)
Central point source:		
RA$_{X-ray}$(J2000)	30°977942	(2)
Dec$_{X-ray}$(J2000)	−4°232405	(2)
$F_{X,[0.5-2]\,keV}$	2.4×10^{-15} erg s^{-1} cm^{-2}	(2)
$F_{X,[2-10]\,keV}$	undetected	(2)
$L_{X,[0.5-2]\,keV}$	1.26×10^{41} erg s^{-1}	(3)
Limit on cluster:		
Count rate	<0.032 ct s^{-1}	(4)
$T_{300\,kpc}$	<1.26 keV	(4)
M_{500}	<5.13×10^{13} $M_\odot$	(4)
L_{500}	<1.76×10^{42} erg s^{-1}	(4)
$F_{X,[0.5-2]\,keV,<300\,kpc}$	<2.82×10^{14} erg s^{-1} cm^{-2}	(4)
$M_{stellar}$	$(2.97 \pm 0.25) \times 10^{11}$ $M_\odot$	(5)
SFR1 (2–20 Myr ago)	0 $M_\odot$ yr^{-1}	(5)
SFR2 (20–600 Myr ago)	1.48 $M_\odot$ yr^{-1}	(5)
SFR3 (0.6–5.6 Gyr ago)	33.08 $M_\odot$ yr^{-1}	(5)
SFR4 (>5.6 Gyr ago)	42.36 $M_\odot$ yr^{-1}	(5)
LW-age	5.7×10^9 yr	(5)
MW-age	7.9×10^9 yr	(5)

Notes. (1) GAMA J020354.47-041356. (2) X-ray point-like source 3XLSS J020354.7-041356 (XXL Paper XXVII). (3) Derived from (2) using our adopted distance. (4) This work. 1σ upper limit on the count rate, converted into limits on flux, mass, and luminosity using scaling relations of XXL Paper IV and XXL Paper XX. (5) This work. SFR refers to the star formation rate in four different periods, derived from model-fitting the GAMA spectrum. LW and MW refer to the luminosity-weighted and the mass-weighted ages.

above the threshold of 15 below which sources are considered spurious and not included in the catalog (Chiappetti et al. 2018).

4.2. Host cluster/group

In the following we review the information that can be gathered from X-ray and optical observations on the possible existence of a cluster or group around the Double Irony.

– X-ray. No cluster is listed at the location of the Double Irony radio galaxy in the new XXL catalog of X-ray detected clusters (XXL Paper XX). From the 1σ upper limit on the count rate within a radius of 300 kpc, we were able to place an upper limit on the X-ray flux, temperature, and luminosity within a radius r_{500} using scaling relations established for XXL clusters (see Table 5): a cluster/group around the Double Irony would have a temperature lower than 1.3 keV and a mass within r_{500} lower than 5.1×10^{13} $M_\odot$. This is significantly lower than the corresponding values measured for the Exemplar's cluster.

A closer inspection of the X-ray image (Fig. 5) does not reveal any clear extended emission. The noise varies across the image and the quality of the data does not allow us to say anything about the presence or absence of gas interaction with the radio lobes.

– Optical. A search in the GAMA database led to the identification of 32 galaxies with spectroscopic redshifts in the $0.13 \leq z \leq 0.15$ range and within a radius of 6.3′ (0.92 Mpc) of the core
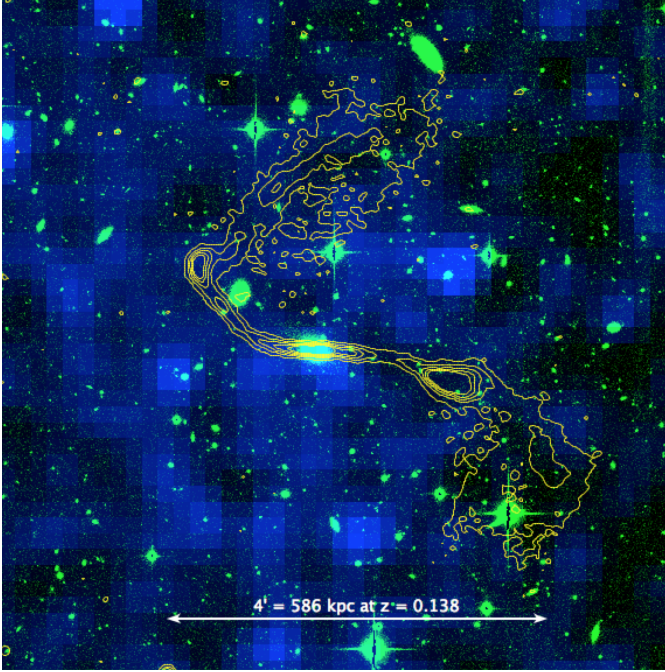
Fig. 5. Multiband false-color image of the Double Irony: X-ray emission in blue displayed at the noise level, optical emission (*i*-band image from the CFHT) in green, radio emission from the GMRT at 610 MHz as yellow contours.

of the Double Irony. This radius was chosen as it corresponds to r_{200} (which is approximately the virial radius) of the Exemplar galaxy cluster. The actual virial radius of the Double Irony galaxy might be different, but this shows that the radio galaxy is surrounded by a large number of galaxies. In Fig. 9 we show the GMRT 610 MHz image of the Double Irony radio galaxy in red, superimposed on an optical *i*-band image from the CFHT in blue. The yellow circles indicate the positions of some of the galaxies in the field cataloged in the GAMA survey; their spectroscopic redshifts are also indicated. We defer the analysis of the spectroscopic redshifts to Sect. 5.3 (cluster mass estimates) and Sect. 5.5 (study of the anisotropy of the surrounding galaxy distribution).

4.3. Radio

4.3.1. Radio morphology

In Fig. 6 we show the radio images of the Double Irony. The structure of the source is best seen in the GMRT 610 MHz image that combines high angular resolution and good sensitivity[20]. The yellow cross indicates the location of the center of the host galaxy. Several features appear clearly in this image: the central east–west jets, a bright lobe to the southwest, a diffuse plume farther out (SW2), a bright region to the northeast (known as the "Elbow"), and a second diffuse plume-like feature to the north that breaks into several lumps. These five main features are also seen in the lower resolution (45″) 1.4 GHz image from the NVSS. The higher resolution FIRST image at the same frequency is badly affected by stripes that prevent us from seeing the two plumes in the north and the southwest. The

---

[20] The Double Irony lies in the northwestern corner of the GMRT 610 MHz mosaic at the intersection of two pointings where the noise is slightly higher than average (see Fig. 5 of XXL Paper XXIX).

TGSS ADR1 image is noisy as well. Only the lobe in the SW1 region is clearly visible. While the lumps of emission in the north and in the Elbow are discernible, it is clear that flux measurements in these regions are affected by the artifacts from the imaging.

Most striking perhaps are the multiple bends: on the eastern side the nearly horizontal jet turns abruptly, but remains collimated until the bright Elbow; the continued structure to the north of the Elbow is fainter and at about 90 degrees from its original direction. On the SW side, the jet shows a small deviation before entering the SW1 lobe, and the SW2 plume is at another angle. The entire structure covers about 4′ and shows a remarkable symmetry by rotation of 180 degrees, which suggests that it is not a superposition of several sources, but forms one system. We examined optical images and could not find any counterparts to the individual features described above.

The XXL-GMRT-610 MHz catalog[21] lists seven resolved sources within 4′ of the core of the Double Irony (XXL Paper XXIX).

Figure 7 shows the GMRT 610 MHz intensity gradient map. The white line (which corresponds to the peaks in the intensity map where the gradient is zero) extends far out and traces the path of the jets. Areas of strong gradients in the inner region and in the Elbow region have a flatter spectral index (Table 7). This has been observed in more nearby low-luminosity FR I radio galaxies by Laing et al. (2011).

Following the jet's path out to the 5σ contour of the GMRT 610 MHz map, we measure a total length of ~7′.56, which corresponds to a projected physical size of 1100 kpc. *This means that the Double Irony is a GRG.*

4.3.2. Luminosity, flux density, spectral index

From the NVSS flux density measurement (Table 5) we derive a spectral luminosity at 1.4 GHz of 6.9×10^{24} W Hz^{-1} (Eq. (3)), or of 2.9×10^{25} W Hz^{-1} at 178 MHz assuming a spectral index of -0.7. This is about twice the spectral luminosity of the *Exemplar*, but still in the range of luminosities of FR I radio galaxies. Some GRGs are powerful radio galaxies with FR II structures (e.g., Subrahmanyan et al. 1996; Ishwara-Chandra & Saikia 1999; Machalski et al. 2001); as the sensitivity of observations increases, more FR I GRGs (or hybrid FR I/FR II) with lobes of lower surface brightness are found (e.g., Lara et al. 2001a; Saripalli et al. 2005).

In Tables 6 and 7 we list the values for the flux densities and the spectral indices measured in different regions displayed in Fig. 6. The spectral indices measured between 150 MHz and 1.4 GHz are systematically steeper than the low-frequency spectral indices measured between 150 and 610 MHz, an indication of spectral aging of the cosmic-ray electrons.

The Elbow and the central region both have a relatively flat spectral index, but no systematic pattern is seen. We intend to model the evolution of cosmic-ray electrons in the Double Irony and in the Exemplar and to derive spectral age estimates by analyzing more sensitive low-frequency data (pending GMRT observations below 500 MHz).

---

[21] Seven sources are listed as resolved in the XXL-GMRT-610 MHz catalog (Smolcic et al. 2018) within 4′ of the core of the Double Irony: XXL-GMRT J020354.8-041356, XXL-GMRT J020353.0-041358, XXL-GMRT J020357.6-041244, XXL-GMRT J020359.1-041303, XXL-GMRT J020348.5-041416, XXL-GMRT J020356.1-041216, and XXL-GMRT J020344.7-041505.
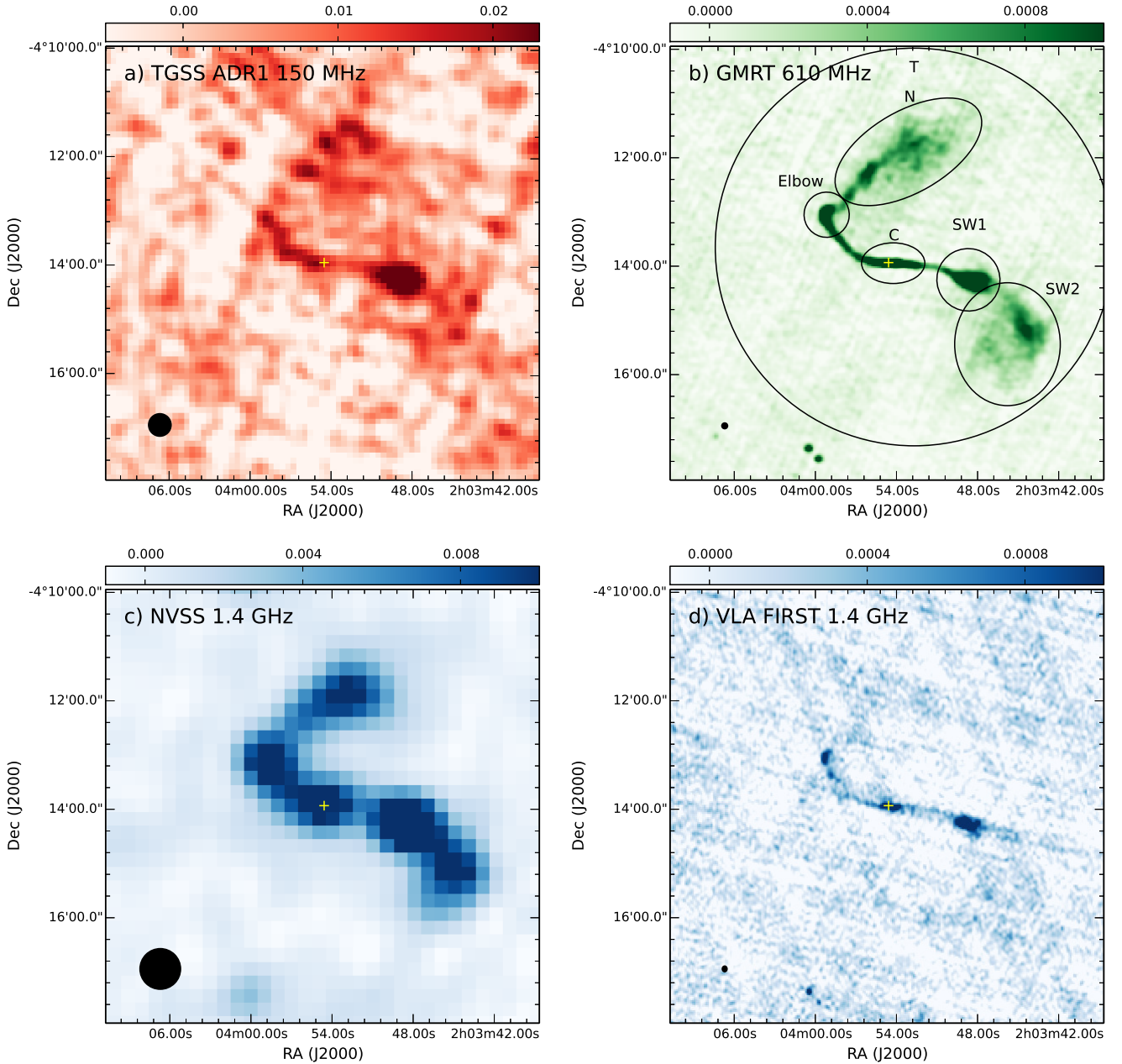
Fig. 6. Radio continuum images of the Double Irony: *a*) from the TGSS ADR1 at 150 MHz; *b*) from the GMRT at 610 MHz; *c*) from the NVSS at 1.4 GHz; *d*) from FIRST at 1.4 GHz. For each image the size of the beam is indicated in the bottom left corner. The cross shows the position of the host galaxy. The northern region (N) is an ellipse of semimajor axis of 90″, semiminor axis of 45″, position angle of −60° from the north, centered at (30°.97133, −4°.19817). The Elbow region is a circular aperture of radius 25″, centered at (30°.99652, −4°.21751). The central aperture (C) is an ellipse of semimajor axis of 35″, semiminor axis of 22″.5, position angle of −55° from the north, centered at (30°.97601, −4°.23241). The SW1 aperture is an ellipse of semimajor axis of 34″.935, a semiminor axis of 34″.551, position angle of −255° from the north, centered at (30°.95282, −4°.237526). The SW2 aperture is an ellipse of semimajor axis of 68″.025, semiminor axis of 58″.426, position angle of 0°, centered at (30°.94079, −4°.2573). The region used for the total flux measured (T) is a circle of radius of 220″, centered at (30°.96956, −4°.2274).

4.3.3. Polarization

Figure 8 shows images of the polarization detected by NVSS[22] at 1.4 GHz. The left panel shows the polarized intensity image overlaid with vectors showing the direction of the electric field of the polarized wave rotated by 90°. In the absence of Faraday rotation, this would correspond to the direction of the magnetic field component on the plane of the sky, $B_\perp$, in the source. The length of the vectors is proportional to the fractional polarization.

The vectors follow the large-scale distribution of the total intensity rather well, except in the very center where they are almost perpendicular to the direction of the inner jets and may trace a poloidal magnetic field. We note, however, that one vector per pixel is shown, so the vectors (like the pixels) are correlated, and variations on scales smaller than the synthesized beam (45″, shown in the bottom left corner) are smoothed out.

---

[22] Four continuum sources associated with the Double Irony are listed in the NVSS catalog (Condon et al. 1998); all of them are listed as polarized, with polarized flux densities ranging from 1.71 to 5.95 mJy. None of these sources appears in the NVSS rotation measure (RM) catalog of Taylor et al. (2009), which had a selection threshold of 5 mJy on the Stokes *I* intensity and of 8σ on the polarized intensity.

Table 6. Flux density measurements in the regions of the Double Irony shown in Fig. 6.

Region	$S_{150\,MHz}$ (mJy)	$S_{610\,MHz}$ (mJy)	$S_{1.4\,GHz}$ (FIRST) (mJy)	$S_{1.4\,GHz}$ (NVSS) (mJy)
C	31.60 ± 10.06	23.75 ± 0.45	10.95 ± 1.23	11.54 ± 0.84
Elbow	17.09 ± 9.14	20.83 ± 0.40	7.59 ± 1.10	8.67 ± 0.68
N	136.25 ± 23.15	77.76 ± 1.03	7.06 ± 2.79*	29.29 ± 1.82
SW1	98.17 ± 12.54	46.29 ± 0.56	14.43 ± 1.52*	23.98 ± 0.99
SW2	99.51 ± 22.84	63.97 ± 1.02	22.93 ± 2.77*	27.88 ± 1.79
T	434.95 ± 79.70	205.76 ± 3.54	21.57 ± 9.65*	131.23 ± 6.27

Notes. The FIRST values marked by a * are significantly lower than those measured in the NVSS, an indication that extended emission has been filtered out.
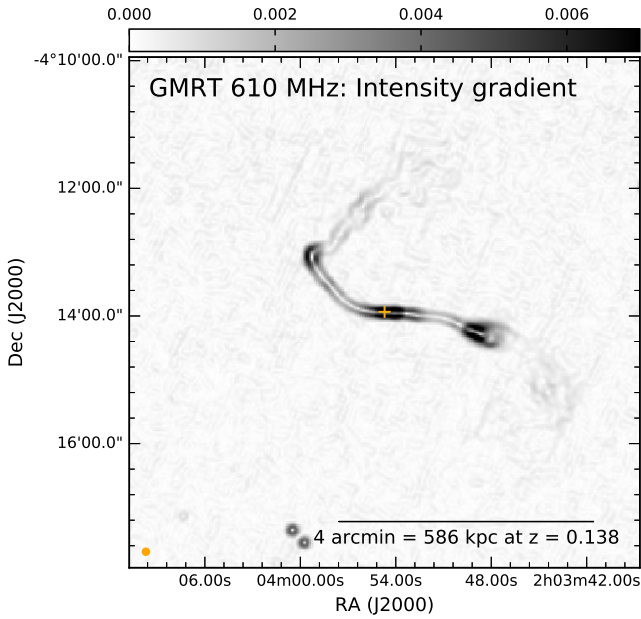
Fig. 7. Grayscale image of the norm of the intensity gradient of the Double Irony at 610 MHz. The path of the jets is clearly visible, in particular the abrupt turn in the region of the Elbow. The beam is shown in the bottom left corner.

Table 7. Spectral index measurements in the different regions of the Double Irony shown in Fig. 6.

| Region	$\alpha^{610\,MHz}_{150\,MHz}$	$\alpha^{1400\,MHz}_{150\,MHz}$
$\Delta\alpha_{sys}$	0.1	0.17
C	−0.20 ± 0.23	−0.45 ± 0.15
Elbow	+0.14 ± 0.38	−0.30 ± 0.24
N	−0.40 ± 0.12	−0.69 ± 0.08
SW1	−0.54 ± 0.09	−0.63 ± 0.06
SW2	−0.31 ± 0.16	−0.57 ± 0.11
T	−0.53 ± 0.13	−0.54 ± 0.08

Notes. At 1.4 GHz the NVSS flux density measurements were used. The first line lists the systematic uncertainties on the spectral indices assuming a 10% systematic uncertainty on the flux densities. The other uncertainties in the table refer to the statistical uncertainties.

In the right panel of Fig. 8 we show an image of the fractional polarization. The position of the core is indicated by a cross. It appears that the fractional polarization peaks on the right side of the core, while the left side is less polarized. This could be a signature of the Laing–Garrington effect (Laing 1988; Garrington et al. 1988): stronger external Faraday depolarization (Burn 1966) occurs along the line of sight of the counter-jet due to the longer path length through a fluctuating magnetic field component. This would mean that the eastern part of jet points away from us, and the more strongly polarized western jet points toward us.

Dedicated observations of the polarization at several radio frequencies are required to map the magnetic field pattern in this radio galaxy and measure the Faraday rotation.

4.4. Nature of the Double Irony

The nature of the Double Irony radio galaxy remains somewhat of a mystery. Given the very large extent on the sky, we suspect that the inclination is not very large, perhaps 30° to 45° relative to the plane of the sky, but the structure is probably not entirely coplanar. The radio galaxy displays a remarkable symmetry by rotation of 180°, except for the strong bend near the Elbow in the northeast, while the western part is more regular.

Similar features have been seen in other FR I radio galaxies. For example 3C 31 has two 90-degree elbows, and the overall radio structure could be nicely reproduced in the dynamical model of an unbound gravitational encounter with a neighboring galaxy (Blandford & Icke 1978). The morphology of the Double Irony is similar to that of NGC 326, a radio galaxy that has been the subject of different interpretations, such as jet precession (Ekers et al. 1978), jet realignment due to gravitational interaction between two galaxies (Wirth et al. 1982), or buoyancy forces that redirect the lobes into regions of lower pressure in the surrounding medium (Worrall et al. 1995). In the following we discuss some physical effects that may have shaped the Double Irony.

4.4.1. A restarted radio galaxy?

Some other GRGs have a morphology that is indicative of a recurrent nuclear activity. For example Saripalli et al. (2002) found an inner double radio structure within larger edge-brightened lobes. The two bright regions of the Double Irony (the SW lobe and the Elbow) and the two diffuse outer plumes beyond the SW lobe and the Elbow may be due to two separate events, where the two brighter inner features would be more recent. However, it would be a coincidence for the restarting lobes to have just reached the bends. It seems more likely that it is a quasi-steady structure influenced by the intergalactic medium.
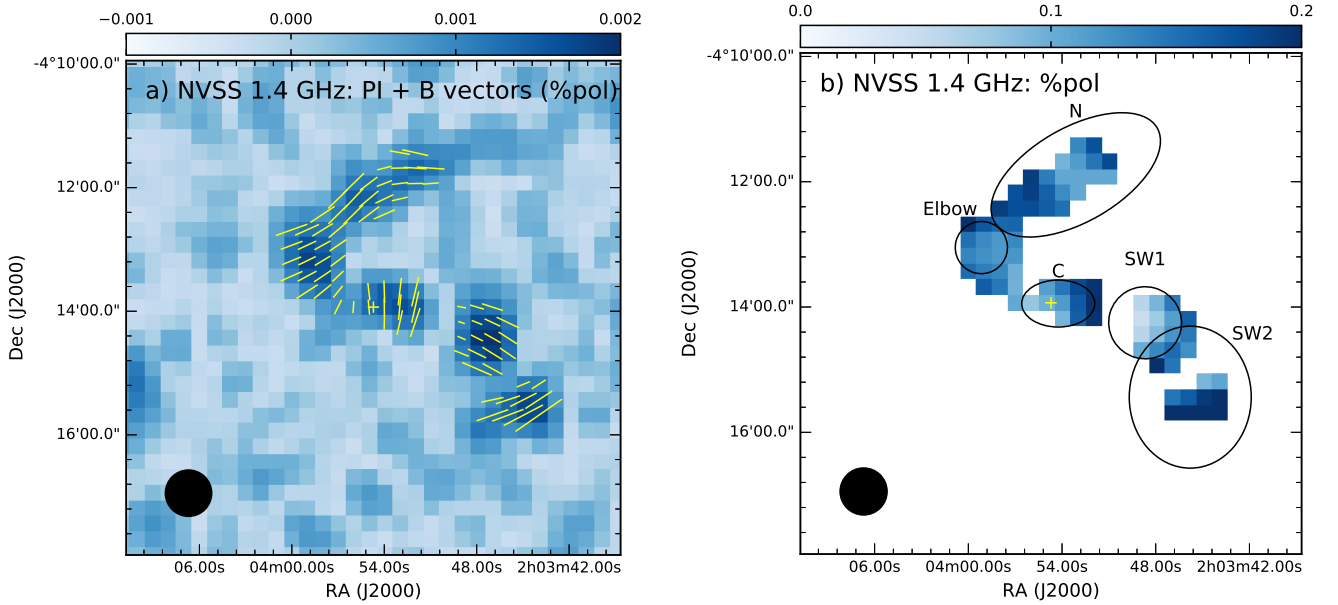
Fig. 8. Polarization in the Double Irony at 1.4 GHz (NVSS). *a*) Polarized intensity image from the NVSS at 1.4 GHz (in Jy beam^{-1}) with vectors indicating the orientation of the electric field of the polarized wave rotated by 90°. The length of the vectors is proportional to the fractional polarization, and 15″ corresponds to a polarized fraction of 10%. In the calculation of the fractional polarization, a threshold of 4.5 mJy beam^{-1} (10σ) was used in total intensity and of 0.8 mJy beam^{-1} (2σ) in polarized intensity. The pixels are not independent: the FWHM of the beam is 45″ and the pixel size is 15″, and vectors are shown for every pixel above the threshold in fractional polarization. *b*) Image of the fractional polarization. The color scale ranges from 0% to 20%. The ellipses correspond to the regions shown in Fig. 6. The highest fractional polarization is found in the southwestern plume. The western jet is more polarized than the eastern one, which might be an indication that the eastern jet points away from the observer and is depolarized (Laing–Garrington effect), while the western jet is directed toward the observer. In both figures the yellow crosses indicate the location of the center of the host galaxy, and the beam is displayed in the bottom left corner.

4.4.2. Gravitational interaction with the second brightest galaxy

A second galaxy is clearly visible to the NE of the host of the Double Irony. It is the next brightest galaxy within a radius of 1 Mpc and is listed in SDSS (SDSS J020357.62–041321.5). With a spectroscopic redshift (from BOSS) of 0.13433, the line-of-sight velocity difference with the host of the Double Irony is 840 km s^{-1}. It is at a distance on the sky of 59″, or a projected distance of 146 kpc. An analysis of the spectrum in the GAMA database (GAMA J20357.62–041321.5) yields a stellar mass of about $0.9 \times 10^{11} \, M_\odot$, which is about one-third of the stellar mass of the host of the Double Irony (Table 5). There is no sign of tidal perturbations in the optical surface brightness distribution of this galaxy, which is an argument against a prograde encounter with the host of the Double Irony. Nevertheless, given the relative line-of-sight velocity difference and their projected distance, the two galaxies could have been interacting gravitationally in the past ∼100 Myr, causing a motion of the host of the Double Irony in the general direction of the second galaxy during the lifetime of the radio source. The drop-like morphology of the SW1 radio lobe is consistent with a global motion of the AGN of the Double Irony toward the east, in the general direction of the companion.

An observation of the distribution of atomic hydrogen via the H I 21 cm line in the companion galaxy may reveal a possible interaction between the two galaxies. The galaxy must contain some atomic hydrogen gas since it is disk-like and star forming: from the GAMA spectrum, we estimated a SFR of about 0.8 $M_\odot$ yr^{-1} in the last 2–20 Myr and a higher SFR earlier (8.8 $M_\odot$ yr^{-1} 20–600 Myr ago and about 19 $M_\odot$ yr^{-1} 0.6–5.6 Gyr ago). The detection of H I tidal tails would constrain the dynamical history of this galaxy. Unfortunately, its redshift places the H I line near 1250 MHz, in a region that is usually affected by radio-frequency interference.

### 4.4.3. Interaction with the gaseous environment

In the absence of a deeper X-ray image not much can be said about the surrounding medium of the Double Irony. The upper limit on the X-ray emission provides an upper limit on the temperature of about 1.3 keV and a limit on the mass within r_{500} of about $5 \times 10^{13} \, M_\odot$ (Table 5). The ejected radio-emitting plasma may have been able to travel farther out because of the low-density of the surrounding medium. The absence of significant X-ray emission may also indicate that the atmosphere of the cluster/group has been so spread out by the radio galaxy's heating and pushing that the $n^2 L$ (density squared times pathlength) through the cluster has dropped from what it was when the radio source turned on. The change in direction of the outer plumes may also be a sign of backflow, as seen for instance in the FR I radio galaxies 3C 296 (Laing et al. 2006), 3C 270 (Kolokythas et al. 2015), or NGC 326 (Hodges-Kluck & Reynolds 2012).

The circumgalactic medium (the gas located outside the optical body of a galaxy but inside the galaxy's virial radius) extends in some cases on scales larger than 100 kpc (Tumlinson et al. 2017) and the Double Irony may have interacted with the circumgalactic medium of its bright neighbor located beyond the bend and mentioned in the previous section.

5. Comparison of the two radio galaxies

In Sect. 6 we show that the Double Irony and the Exemplar are part of the same large-scale structure, a supercluster at $z \simeq 0.14$. In this context it is of interest to compare the two radio galaxies and their environments.

In Sect. 5.1 we estimate their black hole masses from scaling relations. In Sect. 5.2 we discuss the properties of the optical spectra of the host galaxies in relation to what is known from
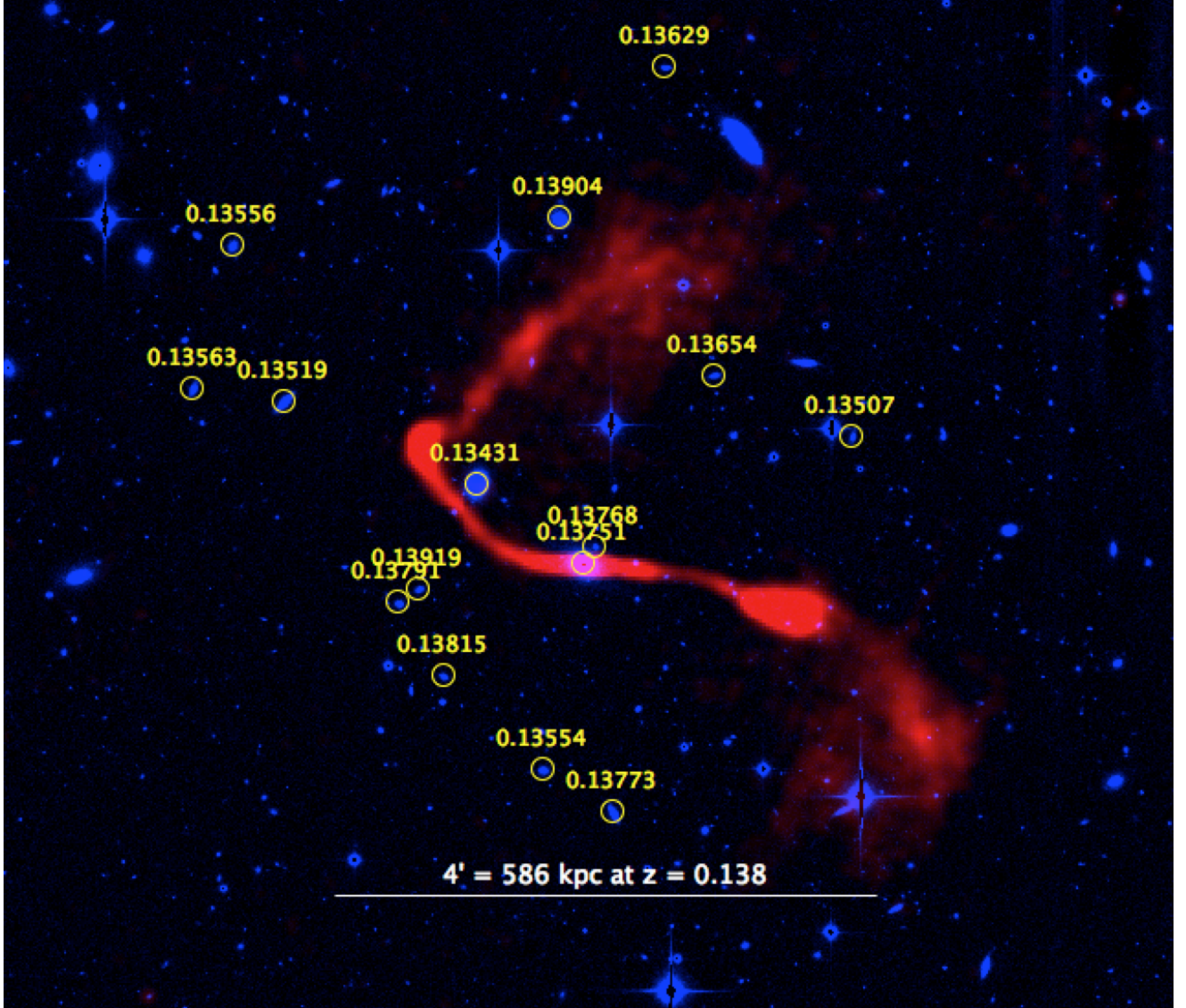
Fig. 9. Multiband false-color image of the Double Irony: *i*-band image from the CFHT in blue, GMRT 610 MHz image in red. The galaxies at a redshift close to that of the host of the Double Irony are shown as yellow circles labeled by their spectroscopic redshift from the GAMA database.

large samples of radio galaxies. In Sect. 5.3 we analyze the distribution of galaxies surrounding the radio galaxies and make estimates of the cluster/group masses. In Sect. 5.4 we derive an age estimate from the properties of the two brightest galaxies in each cluster/group. Finally, in Sect. 5.5 we examine the distributions of galaxies that surround each radio galaxy and quantify their degrees of anisotropy in relation to the orientation of the radio jets and lobes.

5.1. Estimation of the black hole masses

There is a well-known correlation between the mass of the black hole and the stellar mass (bulge mass) of the host galaxy (e.g., Ferrarese & Merritt 2000). This correlation is expressed as

$$\log_{10}\left(\frac{M_{\mathrm{BH}}}{M_\odot}\right) = a + b \log_{10}(X), \tag{4}$$

where X is the stellar mass itself or an indicator of it (e.g., the velocity dispersion, the K-band absolute magnitude).

We have stellar mass estimates for both galaxies (Tables 2 and 5). Using the parameters given by McConnell & Ma

(2013) in their fits to the stellar mass–black hole mass relation ($a = 8.56 \pm 0.10$; $b = 1.34 \pm 0.15$), we obtain

$$
\begin{aligned}
M_{\mathrm{BH}}^{\mathrm{Exemplar}} &\simeq 1.0 \times 10^9 M_\odot \\
M_{\mathrm{BH}}^{\mathrm{Double\ Irony}} &\simeq 1.6 \times 10^9 M_\odot .
\end{aligned}
\tag{5}
$$

For the Exemplar we can also use the value of the velocity dispersion from SDSS DR 14 (Table 2). The fits of McConnell & Ma (2013) for elliptical galaxies when X is the velocity dispersion in units of 200 km s^{-1} have the following parameters: $a = 8.39 \pm 0.06$ and $b = 5.20 \pm 0.36$. This gives a black hole mass of about $1.5 \times 10^9 M_\odot$.

We see that the black holes of the Double Irony and Exemplar both have a mass on the order of $10^9 M_\odot$.

5.2. Brightest cluster galaxies

The host galaxy of the Double Irony is somewhat brighter than that of the Exemplar in all bands except the WISE W1 and W2 bands (the difference is largest in the *u* band, Tables A.2 and A.1).

Table 8. Mass estimates of the clusters.

	Exemplar	Double Irony	Note
$N(R < 6\farcm3)$	46	55	(1)
$N(<6\farcm3, 0.13 < z < 0.15)$	23	32	(2)
z_{cluster}	0.1387	0.1368	(3)
$\sigma_v[\text{km s}^{-1}]$	475	275	(4)
$M_{\text{Caustic}}[M_\odot]$	3.2×10^{14}	9.1×10^{13}	(5)
$M_{200}[M_\odot]$	1.7×10^{14}	3.3×10^{13}	(6)
$M_{500}[M_\odot]$	1.3×10^{14}	2.5×10^{13}	(7)
$M_{500}^{MT}[M_\odot]$	$(0.9 \pm 0.4) \times 10^{14}$	$<5.1 \times 10^{13}$	(8)

Notes. (1) Total number of galaxies within a radius 6.3′ of the cluster center. (2) Number of galaxies within a radius 6.3′ of the cluster center and with $0.13 < z < 0.15$. (3) Redshift estimate of the cluster. (4) Velocity dispersion estimated via the gapper method (Eq. 8). (5) Mass derived via the caustic method. (6) Mass within r_{200} derived via the mass–σ_{200} scaling relation (Eq. 9). (7) Mass within r_{500} scaled from M_{200} estimated via the scaling relation (Eq. 11). (8) Mass within r_{500} derived from X-rays (Table 2 for the Exemplar, and upper limit for the Double Irony, Table 5). The caustic mass estimates are higher than those derived via a simple scaling relation between the mass and the velocity dispersion, and also higher than those derived from X-rays. This apparent discrepancy is not surprising given the relatively small number of galaxies within the structures.

The two host galaxies have very similar optical spectra (Fig. A.1) characteristic of old stellar populations. Detection of Hα, Hβ, and [OII] is reported in the GAMA database for both galaxies. However, there is no detection of high-excitation emission lines such as [OIII] that is seen in the host galaxies of high-excitation radio galaxies (HERGs). It has been shown that the most luminous radio galaxies (FR II) are predominantly HERGs, while the hosts of the less powerful FR I radio galaxies do not exhibit such spectral lines. Low-excitation radio galaxies (LERGs) are in general hosted by galaxies that have a lower star formation rate, are located in clusters, and are more massive than the host galaxies of HERGs. They are believed to have different modes of accreting gas: the LERGs accrete mostly hot gas, whereas the HERGs accrete cold gas and radiate more efficiently (e.g., Hardcastle et al. 2007; Tasse et al. 2008; Smolčić 2009; Best & Heckman 2012; Best et al. 2014). The Exemplar and the Double Irony can both be classified as LERGs.

Both radio galaxies can be classified as FR I from their morphologies. By examining the mid-infrared photometry and colors of the host galaxies of radio galaxies, Sadler et al. (2014) was able to show that FR I and FR II fall in different parts of the (W1-W2)–(W2-W3) color–color diagram (([3.4 μm]–[4.6 μm]–([4.6 μm]–[12 μm]), their Fig. 13). The WISE colors of the hosts of our radio galaxies are consistent with those of FR I radio galaxies (Table A.1).

5.3. Mass of the clusters

The spectroscopic redshifts obtained from the GAMA database allow us to obtain a new mass estimate of the galaxy cluster that hosts the Exemplar, and to search for a cluster/group of galaxies around the Double Irony. The velocities v_i in the rest frame of a cluster at redshift z_{cluster} are simply

$$v_i = c \frac{z_i - z_{\text{cluster}}}{1 + z_{\text{cluster}}}, \qquad (6)$$

where z_i are the redshifts of the galaxies.

The velocity dispersion within the virial radius can be used to obtain an estimate of the virial mass. However, this mass estimate relies on a single number and does not take into account the full distribution of galaxies on the sky and in redshift space. A more sophisticated method is the caustic method developed by Diaferio & Geller (1997) and Diaferio (1999). The idea is to estimate the group's escape velocity from the characteristic

trumpet shape of the distribution of galaxies in the plane defined by the group/cluster-centric distance and the line-of-sight velocities with respect to the median recession velocity of the group. We used the modified caustic mass estimation algorithm written by Alpaslan et al. (2012) to calculate the total masses of galaxy groups in the GAMA group catalog (G^{3}Cv1; Robotham et al. 2011).

5.3.1. Cluster/group membership

The first step is to identify the member galaxies of our two clusters/ groups. We simply selected all the galaxies located within an estimated radius (which corresponds to r_{200} for the Exemplar's cluster) and within a certain spectroscopic redshift range:

$$\begin{cases} R < r_{200} = r_{500}/0.7 = 6.3' = 934 \text{ kpc} \\ 0.13 < z < 0.15 \,. \end{cases}$$

To estimate the radius r_{200}, we used the relation of Ettori & Balestra (2009): $r_{200} = r_{500}/0.7$, which gives $r_{200} = 934$ kpc $= 6\farcm3$ for the Exemplar's cluster, using the value of r_{500} given in Table 2. In the absence of other information on the Double Irony, we took the same value of r_{200} as for the Exemplar. The number of galaxies selected in this manner is given in Table 8. It should be noted that mass estimates depend on how accurately the cluster members have been selected. However, as we see below, the caustic mass method provides a way to assess cluster membership that is complete to a very large degree for massive clusters (Serra & Diaferio 2013).

5.3.2. Caustic mass method

The caustic mass method requires the cluster's redshift and velocity dispersion as inputs in addition to the catalog of positions and redshifts of the individual member galaxies. Rather than using a simple median value and standard deviation, we used the "gapper estimator" introduced by Beers et al. (1990). This estimator has been shown to be unbiased, even for groups with few member galaxies and robust to weak variations in group memberships. The estimated "scale" in velocity space (an estimator of the "velocity dispersion") is calculated as

$$\sigma_{\text{gap}} = \frac{\sqrt{\pi}}{N(N-1)} \sum_{i=1}^{N-1} w_i g_i \,, \qquad (7)$$

where $g_i = v_{i+1} - v_i$ is the velocity difference between each velocity pair computed after having sorted the galaxies' recession velocities in the catalog in increasing order; the weights are $w_i = i(N - i)$, where N is the number of galaxy redshifts and i varies between 1 and $N - 1$.

Following Robotham et al. (2011), we increased the velocity dispersion by a factor $\sqrt{N/(N-1)}$ to take into account the fact that the central galaxy is moving with the center of mass of the halo (associated cluster); we also corrected for the measurement uncertainties on the recession velocities of the individual galaxies (50 km s^{-1} for GAMA; Driver et al. 2011) by subtracting the contribution for the N galaxies in the cluster ($\sigma_{\text{err}} = 50\sqrt{N}$ km s^{-1}):

$$\sigma = \left(\frac{N}{N-1}\sigma_{\text{gap}}^2 - \sigma_{\text{err}}^2\right)^{1/2}. \tag{8}$$

For the Exemplar we used the position of the BCG as the central position. For the Double Irony we used the position of the host galaxy, which is also the brightest galaxy within a radius of about 1 Mpc.

In Fig. 10 we show the results of the caustic mass analysis. The dots show the distribution of the galaxies in phase space, and the magenta lines show the caustic lines fitted to the black parabola. The dots outside the caustics are, by definition, beyond the turn-around radius of the cluster and have a velocity that is greater than the escape velocity. The results are summarized in Table 8.

While there are more galaxies in the area around the Double Irony, the estimated mass of the Double Irony cluster is about three times smaller than that of the Exemplar. The caustic mass analysis shows that many galaxies fall outside the caustic line (see Fig. 10), which indicates that they are not cluster members.

5.3.3. Scaling relations

Now let us estimate the mass within r_{200} using a simple scaling relation with the velocity dispersion within the same radius, σ_{200}. Evrard (2004) showed that the following relation is an excellent fit to a wide range of simulated clusters over a wide range of redshifts,

$$M_{200} = \frac{10^{15}h^{-1}M_\odot}{H(z)/H_0}\left(\frac{\sigma_{200}}{1080 \text{ km s}^{-1}}\right)^3, \tag{9}$$

where $H(z)$ is the value of the Hubble parameter at the redshift z of the cluster. This relation is very close to the mass–velocity dispersion relation for a singular isothermal sphere truncated at the virial radius. For such a model in hydrostatic equilibrium, there is a simple relation between mass and temperature (e.g., Voit 2005)

$$k_B T_{200} = (8.2 \text{ keV})\left(\frac{M_{200}}{10^{15}h^{-1} M_\odot}\right)^{2/3}\left(\frac{H(z)}{H_0}\right)^{2/3}, \tag{10}$$

where k_B is the Boltzmann constant and T_{200} is the temperature within r_{200}.

M_{200} and M_{500} are related by the factor

$$M_{500} = M_{200}/1.35 \tag{11}$$

for an appropriate value of the concentration parameter.

The mass estimates are given in Table 8. The caustic mass estimates are somewhat larger than the estimates from a single scaling relation with the velocity dispersion, and from the
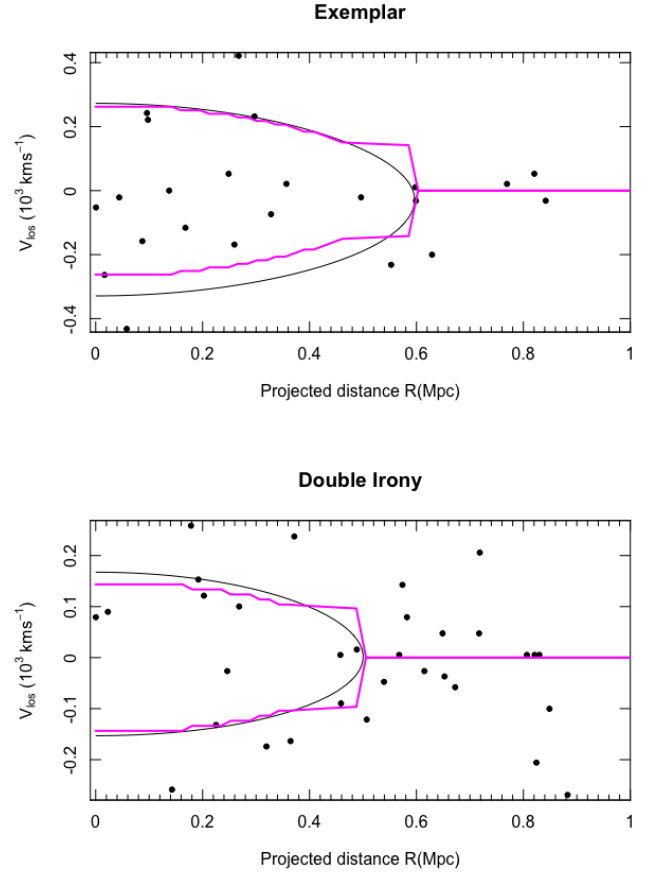

Fig. 10. Result of the caustic mass analysis for the Exemplar (*top panel*) and the Double Irony (*bottom panel*). The dots shows the positions of the galaxies in phase space (R is the distance on the sky to the brightest galaxy, and v_{los} is the line-of-sight velocity relative to the mean line-of-sight velocity of the galaxies in the region. The magenta lines show the caustic lines. Galaxies outside the caustic lines have a v_{los} greater than the escape velocity of the cluster/group.

X-ray derived masses (an upper limit in the case of the Double Irony). Several galaxies in the field of the Double Irony fall outside the caustic line (e.g., the brightest neighbor on the sky has a relatively high velocity relative to the mean velocity of the cluster/group). Given the relatively small number of galaxies, the caustic method may not be reliable to assess cluster membership for individual galaxies. It is also difficult to attach a realistic uncertainty to the caustic mass estimate when the number of galaxies is small. For the GAMA group catalog (G3Cv1), Alpaslan et al. (2012) showed that "on average, the caustic mass estimates agree with dynamical mass estimates within a factor of 2 in about 90% of the groups and compares equally well to velocity dispersion based mass estimates for both high and low multiplicity groups over the full range of masses probed by the G3Cv1". According to all indicators, the cluster/group of the Double Irony is less massive than that of the Exemplar.

The temperature estimates derived from Eq. 10 are 2.1 keV for the Exemplar and 0.7 keV for the Double Irony. These values are consistent with the X-ray estimates ($\approx$1.8 keV for the Exemplar, Table 2; and $\lesssim$1.3 keV for the Double Irony, Table 5).

From the estimates of M_{500} in Table 8, we can estimate that the corresponding radius, r_{500}, for the Double Irony's group is about 0.6 times that of the Exemplar's cluster, or about 380 kpc, which corresponds to 2.'6. A circle of that radius roughly encompasses the entire radio structure.
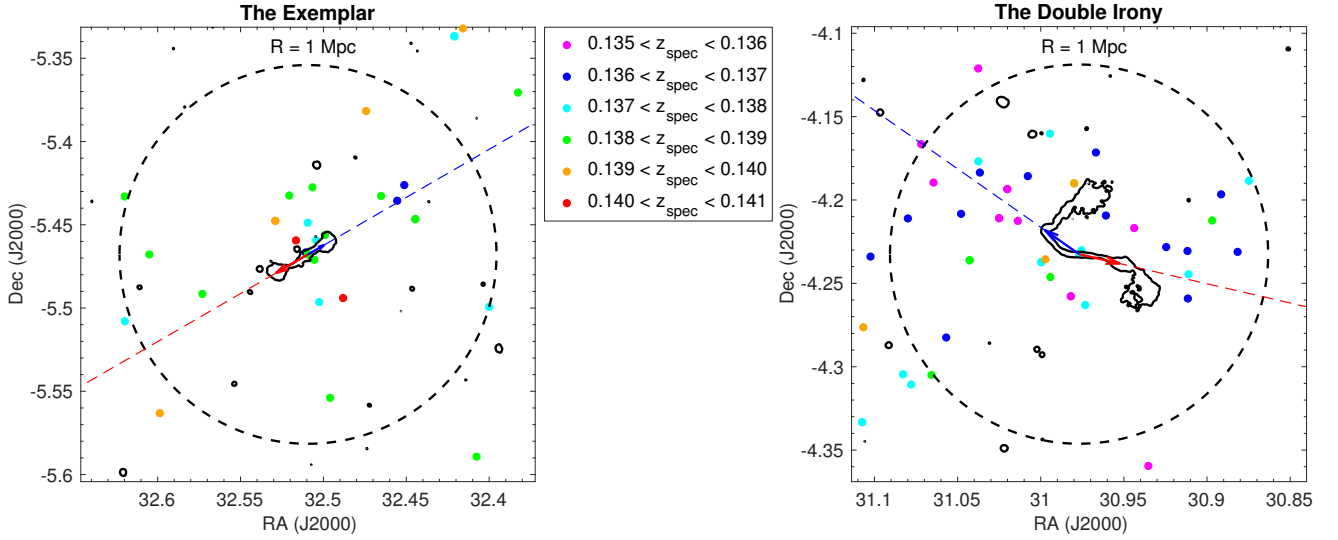
Fig. 11. Distribution of galaxies (colored dots) in the fields of the Exemplar (*left panel*) and of the Double Irony (*right panel*). The dots are color-coded according to the galaxies' spectroscopic redshifts in the GAMA database as indicated by the labels. The black contours correspond to the surface brightness at 610 MHz and increase by a factor of two from 0.3 to 4.8 mJy beam^{-1}. The arrows point toward the brightest areas of the radio lobes; the lines were extended to show the directions of the lobes more clearly. In the Exemplar, the SE lobe is longest (80″ at a position angle of 120° measured from the N toward the E, shown in red); the shorter lobe (40″, blue arrow) points in the opposite direction. In the Double Irony, the arrows point toward the SW lobe (PA = −103°, in red) and toward the NE Elbow (PA = +55° degrees, in blue) and have the same length (90″). Some asymmetries can be seen: more galaxies lie ahead of the shorter (blue) lobe than on the side of the longer lobe in the Exemplar; in the Double Irony, there is an overdensity of galaxies in the NE, beyond the Elbow and the northern plume.

5.4. Cluster ages and dynamical states

The luminosity difference between the BCG and the second brightest galaxy in a cluster is used as an indicator of the evolutionary state of a cluster (e.g., XXL Paper XV). In the hierarchical model of galaxy formation, BCGs located at the center of a cluster will grow by accretion and mergers faster than other galaxies. The difference in mass (and luminosity) is expected to increase with time, and galaxy groups/clusters with a large magnitude difference Δm_{12} between their two brightest galaxies are expected to have assembled early.

Raouf et al. (2014) used galaxies drawn from semi-analytic models of Guo et al. (2011) based on the Millennium simulations, and investigated how some measurable parameters are related to the age of the groups. They defined "young" galaxy groups as those that have assembled up to 30% of their mass by redshift $z = 1$, and "old" groups as the ones that had assembled more than 50% of their mass at redshift $z = 1$. Plotting the distributions of the magnitude gap Δm_{12} versus the absolute magnitude in the r band (M_r) of the BCG, they were able to quantify the fraction of old and young groups in different parts of the diagram.

For the Exemplar's cluster (XLSSC 112), the difference in the r-band magnitude is 0.97, while for the BCG of the Double Irony group it is much lower, 0.35. The second brightest galaxy in the Double Irony environment is a late-type galaxy located near the Elbow radio structure (see Fig. 5 and Sect. 4.4.2). The Exemplar has $M_r = -22.73$ and the Double Irony has $M_r = -22.85$. Placing them in the diagram of Raouf et al. (2014), we see that the Double Irony group has a higher probability of being a young galaxy group (box (3) with 63% probability of being young and 4% probability of being old). The Exemplar group, XLSSC 112, falls in box (7) with a 30% probability of being young and a 22% probability of being old. This means that the probability that the Exemplar's cluster is older that the Double Irony's group/cluster

is 51%, while the probability that the Double Irony is older than the Exemplar is 13%; there is a 36% probability that they are in the same age group (young, old, or in between). While this is not conclusive in itself, it is consistent with the idea that the Double Irony's group/cluster is not as evolved as XLSSC 112.

5.5. Comparing the surrounding galaxy distributions

A number of studies have been carried out to search for a relation between the large-scale distribution of galaxies surrounding GRGs and the orientation of the radio lobes and plumes (e.g., Saripalli et al. 1986; Subrahmanyan et al. 2008; Safouris et al. 2009; Thorat et al. 2013; Malarecki et al. 2015). There is increased evidence that overdensities of galaxies are found on the side of the shorter radio lobes, and that jets are oriented in directions perpendicular to the overall galaxy distribution surrounding the host galaxy; also, non-colinear radio jets and lobes seem to have directions perpendicular to the surrounding galaxy distribution, suggesting that they have been deflected (Malarecki et al. 2015).

XXL-North has been covered by the GAMA spectroscopic survey (G02 region in the GAMA Data Release 3; Baldry et al. 2018) that is 95.5% redshift complete to a magnitude $r < 19.8$ mag. In this section, we begin with a qualitative description of the distribution of galaxies located within a radius of 1 Mpc of the centers of the two radio galaxies and with a spectroscopic redshift from the GAMA database close to that of the radio galaxy (see Fig. 11). Then we carry out a more quantitative analysis in terms of Fourier components of the distribution of the galaxies surrounding the radio sources.

In Fig. 11 we show the distribution of the galaxies with a spectroscopic redshift $z_{RG} - \Delta z < z < z_{RG} + \Delta z$, where $z_{RG} = 0.138$ is the redshift of the radio galaxy and $\Delta z = 0.003$. The galaxies are color-coded in redshift bins of 0.001, increasing from blue to red. The overlaid contour corresponds to the 5σ

Table 9. Fourier components of the galaxy distribution around the two radio galaxies.

Name	R_{max} (Mpc)	N	n (Mpc^{-3})	$\bar{N}_{env}$	$N/\bar{N}_{env}$	A_2	A_3	A_4	A_5
Exemplar	0.5	15	0.794	1.12	13.3	$\mathbf{-0.337 \pm 0.014}$	-0.086 ± 0.012	$+0.048 \pm 0.012$	$\mathbf{-0.250 \pm 0.015}$
Exemplar	1.0	24	0.318	3.62	6.6	$\mathbf{-0.183 \pm 0.006}$	$\mathbf{-0.188 \pm 0.006}$	-0.017 ± 0.006	$+0.041 \pm 0.007$
Double Irony	0.5	19	1.006	0.75	25.3	$+0.119 \pm 0.009$	$\mathbf{-0.178 \pm 0.009}$	$\mathbf{+0.161 \pm 0.008}$	-0.007 ± 0.010
Double Irony	1.0	38	0.503	3.38	11.3	$\mathbf{+0.187 \pm 0.003}$	$\mathbf{-0.173 \pm 0.003}$	$\mathbf{+0.097 \pm 0.003}$	$\mathbf{+0.261 \pm 0.003}$

Notes. N is the number of galaxies in a cylindrical volume of radius R_{max} and depth of $2\Delta z$, where $\Delta z = 0.003$, centered at the position and redshift of the host galaxy; n is the number density of galaxies in the same volume; $\bar{N}_{env}$ is the average number of galaxies in the environment, calculated in similar volumes placed at eight locations around the radio galaxy (see text). The most significantly detected anisotropy parameters are in bold.

level (0.3 mJy beam^{-1}) in the 610 MHz images of the radio galaxies. The arrows point in the directions of the brightest regions in the lobes. The lines were extended to separate the regions above and below the radio axes.

In the Exemplar, the jets and lobes point in opposite directions, but the SW lobe is farther away from the core than the NE lobe. The red arrow points to the brightest region in the longer lobe and the blue arrow to the shorter one. We note the following:
– more galaxies are clearly situated above the Exemplar's radio axis;
– an overdensity of galaxies are in the direction of the shorter lobe relative to the opposite direction;
– in the central region, the galaxy distribution is roughly perpendicular to the radio axis.
The Double Irony radio galaxy is not a linear structure. The red arrow points to the brightest region in the SW lobe and the blue arrow to the Elbow; these two regions are at about the same distance from the center of the host galaxy (90″), but have different position angles. We see:
– an overdensity of galaxies above the radio axis (at positive angles, measured counterclockwise).
– in the direction of the blue arrow, an overdensity of galaxies beyond the Elbow and to the east of the northern plume;
– an overdensity to the northwest of the SW plume.
To quantify the distribution of the galaxies around our two radio galaxies and those apparent features, let us use the Fourier component method proposed by Thorat et al. (2013) and applied to a sample of GRGs by Malarecki et al. (2015).

The method consists of estimating five components defined as

$$A_1 = \sum_{i=1}^{N} f_k(\theta_i), \tag{12}$$

and

$$A_k = \frac{1}{N} \sum_{i=1}^{N} f_k(\theta_i) \quad \text{for } k = 2, ..., 5, \tag{13}$$

where the summation is over the number of galaxies, N, within a radius R (taken to 0.5 or 1 Mpc) and a redshift $\Delta z = \pm 0.003$ of the position and redshift of the radio galaxy; the values of θ_i are the angles measured counterclockwise on the sky between the direction of galaxy i and that of the longer radio lobe; the f_k functions are $f_1 = 1$, $f_2 = \sin(\theta_i)$, $f_3 = \cos(\theta_i)$, $f_4 = \sin(2\theta_i)$, $f_5 = \cos(2\theta_i)$.

We use a slightly different notation from that of Malarecki et al. (2015; A_k rather than a_k) to make it clear that our A_k are normalized by dividing by the number of galaxies N in

the corresponding volume surrounding the radio galaxy, while Malarecki et al. (2015) divided by the number of galaxies located farther out in the environment of the radio sources. The absolute values of their a_k are therefore a mixture of information related to the actual local anisotropy of the galaxy distribution and the overdensity with respect to the more distant environment. The difference is therefore simply a normalization factor (which is different for every radio galaxy) and we find the use of A_k more intuitive because they are actual mean quantities.

The A_k components are illustrated in Fig. 12 and can be understood as follows:
1. $A_1 = N$ is simply the number of galaxies located within the pre-defined radius from the core of the radio galaxy.
2. A_2 and A_3 are sensitive to a dipolar distribution of galaxies. The A_3 parameter (average of the cosines) is sensitive to asymmetries in the density distribution of galaxies along the radio axis (e.g., a positive A_3 indicates an overdensity of galaxies along the longer radio lobe compared to the opposite direction; a negative A_3 indicates an overdensity along the shorter radio lobe). The A_2 parameter (average of the sines) expresses asymmetries between the two sides of the radio axis (i.e., in the direction perpendicular to that of the radio axis, above or below the radio axis);
3. A_4 and A_5 are sensitive to a quadrupolar distribution. A positive A_5 (average of $\cos(2\theta_i)$) corresponds to overdensities of galaxies along the radio axis compared to the direction perpendicular to the radio axis; a negative A_5 will indicate an overdensity above and below the radio axis compared to along the radio axis. A_4 (average of $\sin(2\theta_i)$ also indicates a quadrupolar anisotropy, but at a 45° angle compared to the previous distribution (see Fig. 12).

In the case of a non-uniform distribution of surrounding galaxies, all A_k components will differ significantly from zero.

The quoted uncertainties on the A_k Fourier coefficients ($k \geq 2$) are standard errors and were calculated using jackknives: the A_k coefficients were recalculated by removing one galaxy at a time; then the standard error on the A_k values was calculated.

To estimate the overdensity of galaxies around the radio galaxy, we defined a 3×3 grid centered on the radio galaxy host at (RA_{RG}, DEC_{RG}) with eight points placed at $RA = RA_{RG} \pm \Delta\theta$ and $DEC = DEC_{RG} \pm \Delta\theta$, with $\theta = 0.5°$. Then we calculated the mean number of galaxies in eight 24 Mpc^3 volumes (radius of 1 Mpc and $z = z_{RG} \pm 0.003$), $\bar{N}_{env}$. The overdensity is $N/\bar{N}_{env}$, where N is the number of galaxies within the same volume centered on the radio galaxy (in the middle of the grid).

The distribution of galaxies with spectroscopic redshifts from the GAMA database close to that of the two radio galaxies is displayed in Fig. 11. The Fourier analysis was applied to this data set and the resulting A_k components are listed in Table 9. The main results can be summarized as follows:
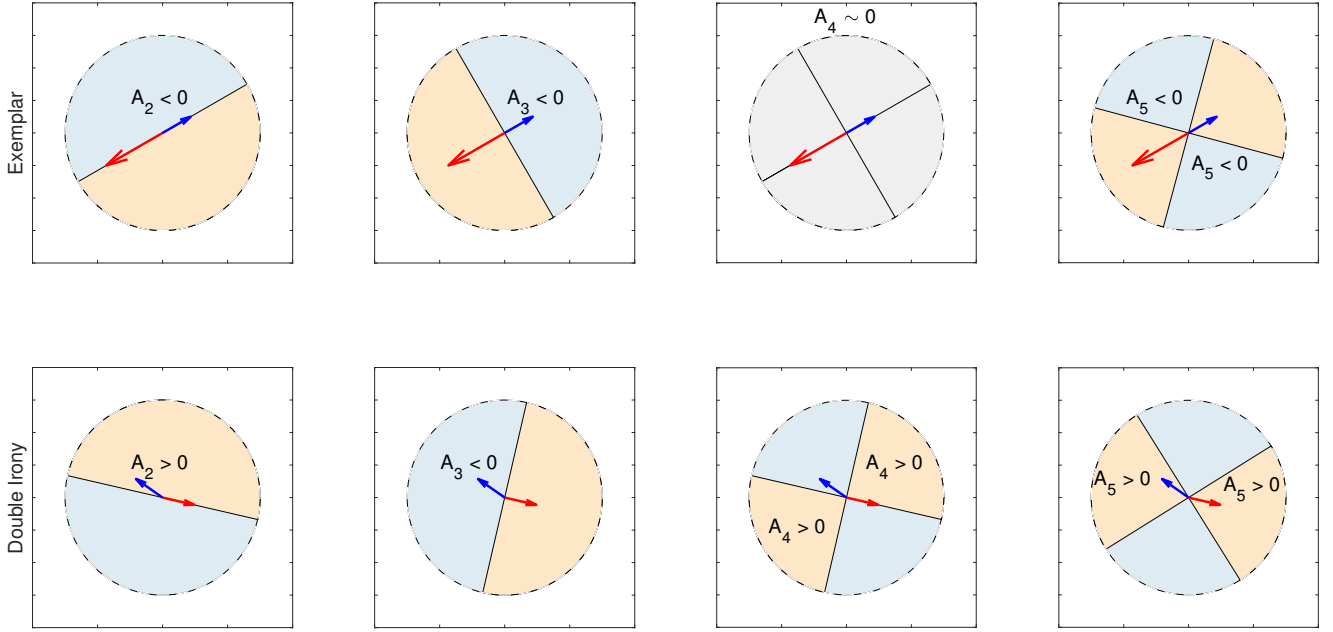
Fig. 12. Illustration of the Fourier components used to quantify the anisotopy in the distribution of galaxies surrounding the Exemplar radio galaxy (*top panel*) and the Double Irony (*bottom panel*). The A_2 and A_3 parameters are sensitive to a dipolar distribution and the A_4 and A_5 to a quadrupolar distribution. The arrows indicate the orientation of the radio jets. For the Exemplar the red arrow shows the direction of the longer radio lobe. In the Double Irony the blue and red arrows have the same length and point toward the brightest regions in the lobes. In the calculation of the A_k parameters, the red arrow (SW lobe) is taken as the origin of the angles θ_i. The blue regions correspond to negative values of the A_k parameters and the orange regions to positive values. In each panel the measured sign of each A_k parameter is indicated in the corresponding region.
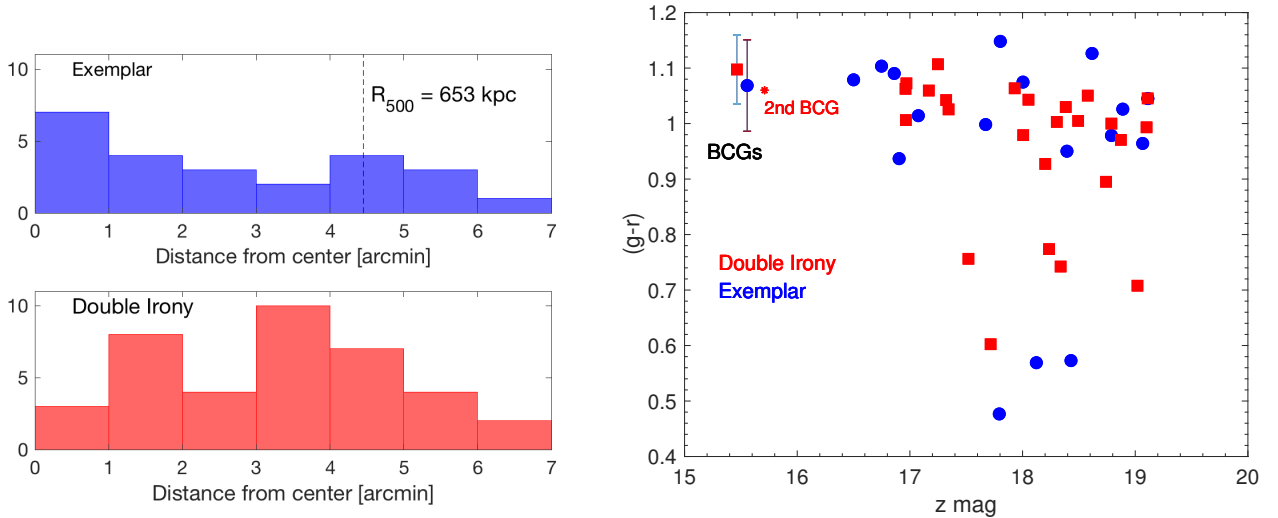
Fig. 13. *Left panel:* histograms of the radial distribution of galaxies with spectroscopic redshifts from GAMA within 7′ (about 1 Mpc) of the host of each radio galaxy and with a spectroscopic redshift within ±0.003 from the redshift of the radio galaxies ($z = 0.138$). The galaxy distribution in the field of the Exemplar is more concentrated than that in the field of the Double Irony. *Right panel:* SDSS color-magnitude diagram of the galaxies located within a radius of 1 Mpc of the host of each radio galaxy and with a spectroscopic redshift within ±0.003 from the redshift of the radio galaxies ($z = 0.138$). Also shown (red star) is the second brightest galaxy located about 1′ to the NE of Double Irony's host and discussed in Sect. 4.4.2. This galaxy has a redshift that falls just below the selected redshift range and is not included in the Fourier component analysis. Except for the presence of the second bright galaxy near the Double Irony, the distributions are very similar (red squares for Double Irony and blue dots for Exemplar).

– N (= A_1) and $N/\bar{N}_{env}$: there are significantly more galaxies within a radius of 1 Mpc of the host of the Double Irony than around the Exemplar. The overdensity compared to the local environment is almost twice as large for the Double Irony as for the Exemplar. Given such a large number of galaxies in the Double Irony, the non-detection of X-ray emitting gas may seem surprising. Could it be that the galaxies around the Double Irony are less massive than in and around the

Exemplar's cluster? To answer this question we retrieved the *ugriz* magnitudes (model magnitudes from SDSS) of the galaxies with spectroscopic redshifts from GAMA. Figure 13 (right panel) is a color-magnitude diagram for both regions. Error bars are shown only for the two BCGs so as not to clutter the figure (the error bars on the *z*-magnitudes are smaller than the widths of the points). The distributions of galaxies in the radio galaxies' environment are similar: most galaxies are red, with a $(g - r)$
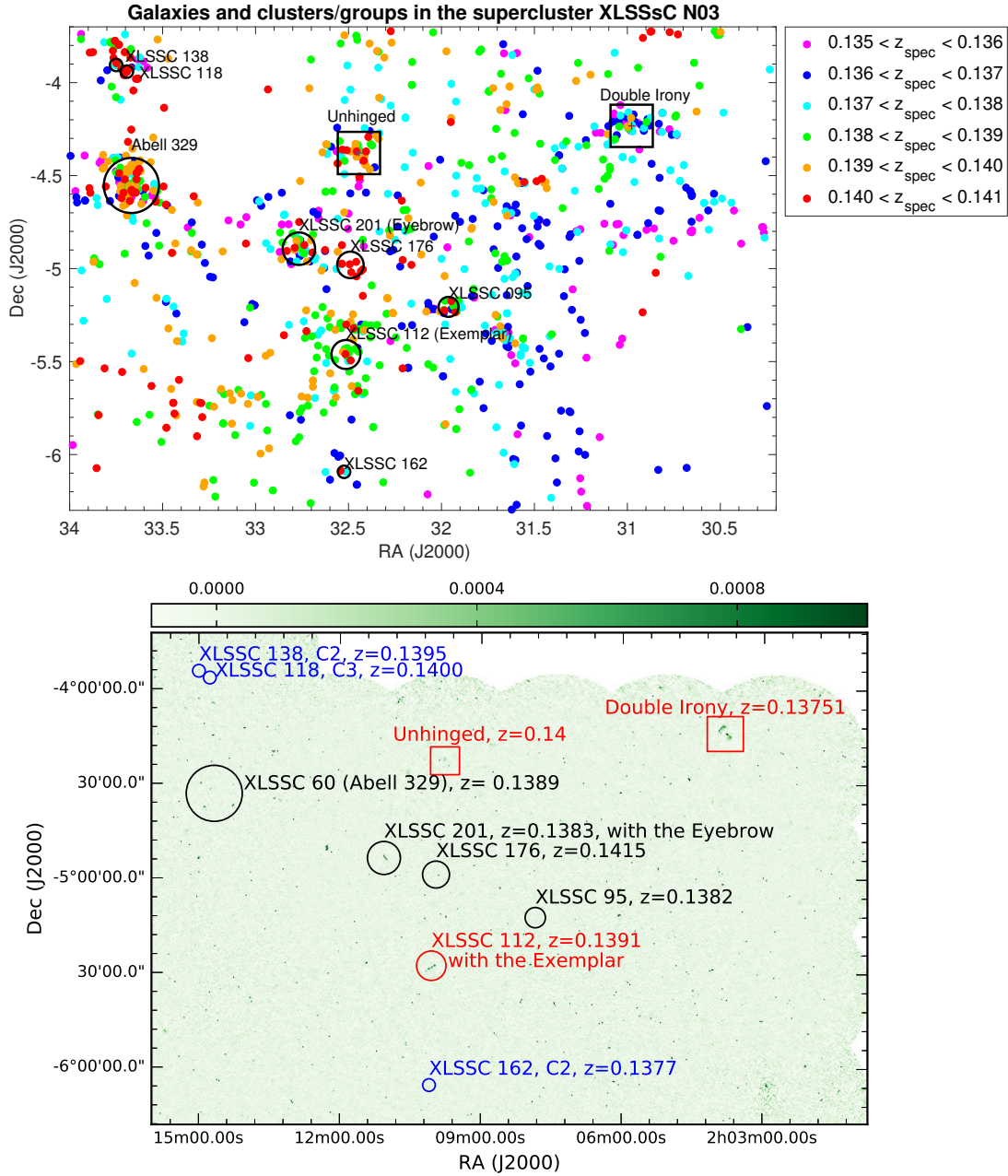
Fig. 14. *Top panel*: distribution of galaxies in the area of the supercluster XLSSsC N03 identified in XXL Paper XX. The galaxies are color-coded according to their spectroscopic redshifts in the GAMA database. The black circles indicate the locations of the eight clusters/groups of galaxies that are known members of the supercluster. The two black squares indicate the location of the newly identified group associated with the Double Irony (in the upper right corner) and that of an overdensity of galaxies where a peculiar radio source (the "Unhinged") is found. *Bottom panel*: GMRT 610 MHz image of the field. As in the upper panel, the size of the black circles indicates the extent (radius r_{500}) of the securely detected XXL clusters (C1 class). The three clusters circled in blue are C2 or C3 clusters whose sizes were not determined (in the C2 sample of XXL clusters, 50% of the sources are likely to be real detections; the C3 sample contains the most uncertain sources). The Double Irony radio galaxy can be seen in the upper right corner inside a square of 1 Mpc on the side. The location of the Unhinged radio source is also indicated by a red square.

color around 1.05. On the *x*-axis we show the *z*-band magnitude which can be used as a proxy for the mass. The two BCGs stand out in the upper left corner of the plot as the brightest (and likely most massive galaxies), with a *z*-band magnitude difference of at least one compared to the other galaxies, except for the second brightest galaxy (marked as a red star) discussed in Sect. 4.4.2 and located about 1′ to the NE of the Double Irony host; we note that this galaxy was not included in the Fourier component analysis because its redshift falls just below the selected redshift interval of 0.138 ± 0.003. The distribution of galaxies is more

concentrated around the Exemplar than around the Double Irony (Fig. 11; left panel of Fig. 13).

– Dipole (A_2 and A_3): $A_2 > 0$ for the Exemplar and <0 for the Double Irony. In both cases this means that there are more galaxies above the radio axes (see Fig. 12; we note that for the Examplar the origin of the angles is taken as the longer lobe (red arrow), directed toward the SE, so the positive A_2 are under the radio axis; this is the opposite for the Double Irony where the red arrow points toward the SW). There is also an anisotropy in the other direction (A_3).
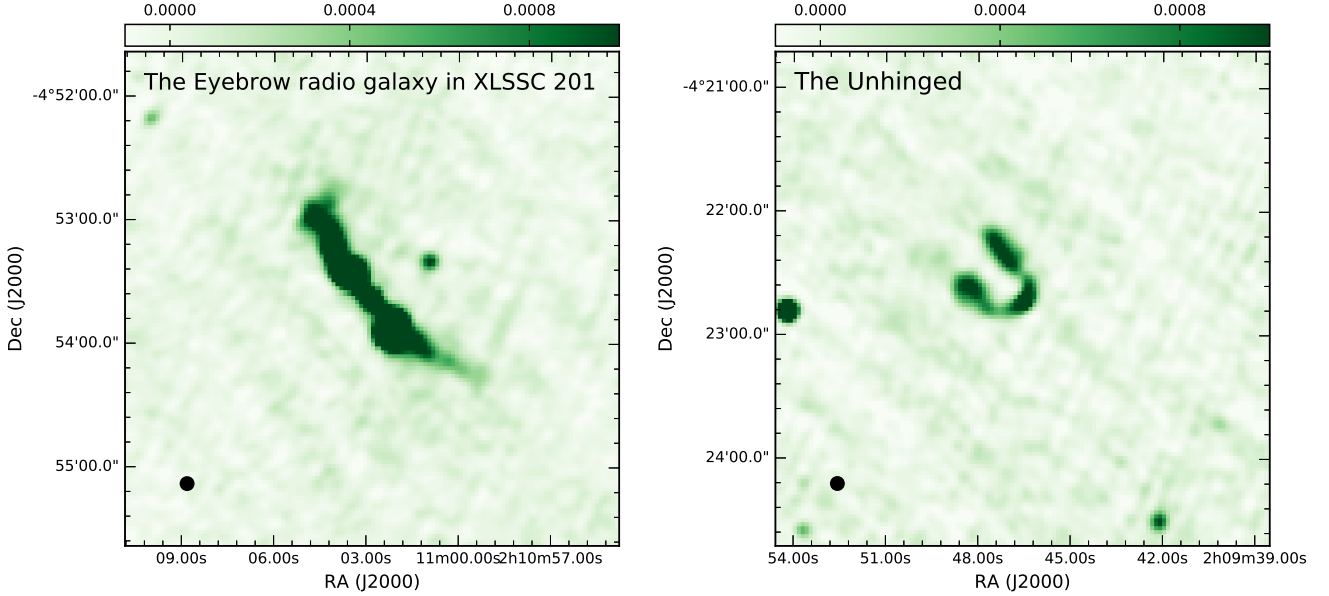
Fig. 15. GMRT 610 MHz images. *Left panel:* radio galaxy located in the cluster XLSSC 201, a known member of the supercluster. There are three radio sources within a radius of 1′ of the center of the figure in the GMRT-XXL-N 610 MHz catalog of Smolcic et al. (2018): XXL-GMRT J021102.8-045338 and XXL-GMRT J021102.9-045335 (same "groupid" 22), and XXL-GMRT J021100.9-045320. *Right panel:* peculiar radio source (possibly a composite) located in the region of a newly discovered overdensity of galaxies in the same supercluster. The grayscale ranges from -10^{-4} to 10^{-3} Jy beam^{-1} and the beam is displayed in the bottom left corner. The GMRT-XXL-N 610 MHz contains four sources within a radius of 1′ at the location of the Unhinged: XXL-GMRT J020946.5-042242, XXL-GMRT J020947.0-042223, XXL-GMRT J020948.1-042240, and XXL-GMRT J020947.5-042213 ("groupid" 157).

– Quadrupole (A_4 and A_5): most interesting are the negative A_5 values for the Exemplar that reflect overdensities in the direction perpendicular to the radio axis, as noted through visual examination. This anisotropy is considerably stronger within a radius of 0.5 Mpc. For the Double Irony, the effect is the opposite: the anisotropy corresponds to overdensities in the direction of the radio axis that corresponds to the orange arrow). Interestingly, the jets seems to be deflected in both directions and redirected into regions of lower galaxy densities (see right panel of Fig. 11).

It seems that the Double Irony radio galaxy has been able to expand and become a GRG in an environment that may not be significantly less dense in galaxies than that of the Exemplar, and has been strongly affected by this environment: the jets deviated from their paths and the lobes expanded away from regions of higher galaxy density into sparser regions.

6. Large-scale structure at *z* = 0.14

In Fig. 14 we show the distribution of the galaxies with a spectroscopic redshift from the GAMA database between 0.135 and 0.141 (top panel) and the GMRT 610 MHz image (bottom panel) of the region of XXL-North that encompasses the supercluster XLSSsC N03 identified in XXL Paper XX. The supercluster contains eight cluster members, five of which are securely detected clusters in X-rays (C1 class). The cluster hosting the Exemplar, XLSSC 112, is a secure X-ray detection and its position is circled in red. There is an interesting alignment on the sky of four clusters, with a decrease in size and mass from the more massive Abell cluster (XLSSC 60) to the other clusters on the right. This large structure might lead to the formation of a massive cluster if infall and merger occur.

The Double Irony radio galaxy is seen in the top right corner of Fig. 14 (left panel). The redshift of its surrounding cluster/group is very similar to the redshifts of the members of the

supercluster ($z \simeq 0.14$). We performed a new friends-of-friends analysis with exactly the same parameters as those used in the study presented in XXL Paper XX, which used 326 clusters with $0.03 < z < 1.0$, but adding the Double Irony's cluster to the list of clusters. Very interestingly, *the Double Irony's cluster was identified as a new member (the ninth) of the supercluster XLSSsC N03*.

We note an overdensity of galaxies at RA $\simeq 32°.445$, DEC $\simeq -4°.38$ (upper panel) where there is no reported XXL cluster. When this structure is added to the list of identified clusters/groups, the friends-of-friends algorithm identifies it as a new member (the tenth) of the same supercluster. Even at this location, a radio source is found in the GMRT 610 MHz mosaic; we call it "the Unhinged" because of its bizarre appearance (see Fig. 15).

7. Radio galaxies in superclusters

We note that XLSSC 201, another cluster member of the supercluster, also hosts an extended radio source, shown in Fig. 15 and denoted the "Eyebrow." It is remarkable that four out of ten clusters/groups in this structure contain well-developed radio galaxies. The Eyebrow and the Unhinged may be the superposition of radio sources at different redshifts and deserve a separate detailed study.

More work is clearly needed to quantify the incidence of radio galaxies in clusters residing inside superclusters. A number of superclusters have been identified in XXL (21 in XXL-North and 14 in XXL-South; XXL Paper XX). Guglielmo et al. (2018b, XXL Paper XXX) characterized the stellar populations of the galaxies in the richest XXL supercluster (at $z \simeq 0.3$) and found evidence for an active role of the environment on the star formation rates and stellar masses. Koulouridis et al. (2016, XXL Paper XII) detected a number of X-ray AGN in three XXL superclusters, but a larger study is needed to reach

firm conclusions on the frequency of AGN in superclusters. The first supercluster detected in XXL is at $z = 0.43$ (Pompei et al. 2016, XXL Paper VII). Its galaxy and AGN populations have been studied in the optical and in the radio, but no large radio galaxies were found within the supercluster's overdensities (Baran et al. 2016, XXL Paper IX). The GMRT-XXL-N 610 MHz survey (XXL Paper XXIX) can be used to search for radio galaxies in superclusters in XXL-North; XXL-South has been covered with the Australia Telescope Compact Array (Butler et al. 2018a,b – XXL Paper XVIII and XXL Paper XXXI, respectively).

In the hierarchical model of structure formation, structures grow by accretion and mergers, small structures forming first. Superclusters of X-ray-detected clusters/groups are large structures that may still be collapsing. Both the AGN of a radio galaxy and its host galaxy (usually a massive elliptical) have accreted significant amounts of material, and the jets and lobes trace the relatively recent (a few 10^7 yr) ejection of plasma. Because of their sizes, radio galaxies are easily seen and might be a powerful way to find new clusters/groups that have escaped detection in X-ray surveys (e.g., Banfield et al. 2016; from the Radio Galaxy Zoo).

8. Summary and conclusion

We have presented an analysis of two radio galaxies at $z \sim 0.14$ identified in the GMRT-XXL-N 610 MHz survey of XXL-North. We have made use of the extensive multiwavelength coverage of XXL to gain a better understanding of those sources. We were able to identify their host galaxies, and in the case of the Exemplar the host cluster that had been detected in the X-ray and cataloged as an XXL cluster. The second and more spectacular source, the Double Irony, is a giant radio galaxy with a linear size of about 1100 kpc on the sky. We were able to show that it is hosted by the BCG of a lower mass cluster with member galaxies detected in the optical and listed in the GAMA database. Using a friends-of-friends algorithm, we were able to show that both clusters are part of the same supercluster. We identified another overdensity of galaxies in the supercluster that is associated with a radio galaxy of peculiar shape. This brings the total number of members of this supercluster to ten. Four of these clusters/group host a radio galaxy. Anisotropies were found in the distribution of the surrounding galaxies, possibly indicating that the jets and lobes/plumes reside in lower density regions. This shows the potential of the XXL survey to lead to the discovery of new structures, and the use of radio galaxies as tracers of large-scale structure.

Future work on the two clusters presented here will require more sensitive, higher angular resolution radio and X-ray data. In particular, the JVLA (including polarization) at GHz frequencies and the GMRT below 500 MHz will allow a detailed modeling of the aging of the cosmic-ray electrons in the radio jets and lobes and will constrain timescales. In the X-ray, a deeper *XMM-Newton* observation of the Double Irony is necessary to detect the hot gas that is likely to be associated with the optically detected group; higher resolution images with *Chandra* may reveal the structure of the gaseous atmosphere around the radio galaxies and possibly shocks.

The XXL fields contain other remarkable radio galaxies that will be analyzed following an approach similar to the one presented here. Special attention will be given to their potential relation to clusters and superclusters.

References

Adami, C., Giles, P., Loulouridis, E., et al. 2018, A&A, 620, A5 (XXL Survey, XX)
Alpaslan, M., Robotham, A. S. G., Driver, S., et al. 2012, MNRAS, 426, 2832
Astropy Collaboration (Robitaille, T. P., et al.) 2013, A&A, 558, A33
Baldry, I. K., Liske, J., Brown, M. J. I., et al. 2018, MNRAS, 474, 3875
Banfield, J. K., Andernach, H., Kapińska, A. D., et al. 2016, MNRAS, 460, 2376
Baran, N., Smolčić, V., Milaković, D., et al. 2016, A&A, 592, A8 (XXL Survey, IX)
Becker, R. H., White, R. L., & Helfand, D. J. 1995, ApJ, 450, 559
Beers, T. C., Flynn, K., & Gebhardt, K. 1990, AJ, 100, 32
Best, P. N., & Heckman, T. M. 2012, MNRAS, 421, 1569
Best, P. N., Ker, L. M., Simpson, C., Rigby, E. E., & Sabater, J. 2014, MNRAS, 445, 955
Blandford, R. D., & Icke, V. 1978, MNRAS, 185, 527
Bock, D. C.-J., Large, M. I., & Sadler, E. M. 1999, AJ, 117, 1578
Burn, B. J. 1966, MNRAS, 133, 67
Butler, A., Huynh, M., Delhaize, J., et al. 2018a, A&A, 620, A3 (XXL Survey, XVIII)
Butler, A., Huynh, M., Delvecchio, I., et al. 2018b, A&A, 620, A16 (XXL Survey, XXXI)
Chabrier, G. 2003, PASP, 115, 763
Chiappetti, L., Fotopoulou, S., Lidman, C., et al. 2018, A&A, 620, A12 (XXL Survey, XXVII)
Clarke, A. O., Heald, G., Jarrett, T., et al. 2017, A&A, 601, A25
Condon, J. J., Cotton, W. D., Greisen, E. W., et al. 1998, AJ, 115, 1693
Croton, D. J., Springel, V., White, S. D. M., et al. 2006, MNRAS, 365, 11
Dabhade, P., Gaikwad, M., Bagchi, J., et al. 2017, MNRAS, 469, 2886

Diaferio, A. 1999, MNRAS, 309, 610

Diaferio, A., & Geller, M. J. 1997, ApJ, 481, 633

Driver, S. P., Hill, D. T., Kelvin, L. S., et al. 2011, MNRAS, 413, 971

Duah Asabere, B., Horellou, C., Jarrett, T. H., & Winkler, H. 2016, A&A, 592, A20

Eckert, D., Ettori, S., Coupon, J., et al. 2016, A&A, 592, A12 (XXL Survey, XIII)

Ekers, R. D., Fanti, R., Lari, C., & Parma, P. 1978, Nature, 276, 588

Ettori, S., & Balestra, I. 2009, A&A, 496, 343

Evrard, A. E. 2004, in Clusters of Galaxies: Probes of Cosmological Structure and galaxy Evolution, eds. J. S. Mulchaey, A. Dressler, & A. Oemler (CUP), 1

Fanaroff, B. L., & Riley, J. M. 1974, MNRAS, 167, 31

Ferrarese, L., & Merritt, D. 2000, ApJ, 539, L9

Fotopoulou, S., Pacaud, F., Paltani, S., et al. 2016, A&A, 592, A5 (XXL Survey, VI)

Fritz, J., Poggianti, B. M., Bettoni, D., et al. 2007, A&A, 470, 137

Garrington, S. T., Leahy, J. P., Conway, R. G., & Laing, R. A. 1988, Nature, 331, 147

Giles, P. A., Maughan, B. J., Pacaud, F., et al. 2016, A&A, 592, A3 (XXL Survey, III)

Guglielmo, V., Poggianti, B. M., Vulcani, B., et al. 2018a, A&A, 620, A7 (XXL Survey, XXII)

Guglielmo, V., Poggianti, B. M., Vulcani, B., et al. 2018b, A&A, 620, A15 (XXL Survey, XXX)

Guo, Q., White, S., Boylan-Kolchin, M., et al. 2011, MNRAS, 413, 101

Gwyn, S. D. J. 2012, AJ, 143, 38

Hardcastle, M., Evans, D., & Croston, J. 2007, MNRAS, 376, 1849

Hardcastle, M. J., Gürkan, G., van Weeren, R. J., et al. 2016, MNRAS, 462, 1910

Heald, G. H., Pizzo, R. F., Orrú, E., et al. 2015, A&A, 582, A123

Helfand, D. J., White, R. L., & Becker, R. H. 2015, ApJ, 801, 26

Hinshaw, G., Larson, D., Komatsu, E., et al. 2013, ApJS, 208, 19

Hodges-Kluck, E. J., & Reynolds, C. S. 2012, ApJ, 746, 167

Hunter, J. D. 2007, Comput. Sci. Eng., 9, 90

Intema, H. T., Jagannathan, P., Mooley, K. P., & Frail, D. A. 2017, A&A, 598, A78

Ishwara-Chandra, C. H., & Saikia, D. J. 1999, MNRAS, 309, 100

Jamrozy, M., Konar, C., Machalski, J., & Saikia, D. J. 2008, MNRAS, 385, 1286

Kolokythas, K., O'Sullivan, E., Giacintucci, S., et al. 2015, MNRAS, 450, 1732

Koulouridis, E., Poggianti, B., Altieri, B., et al. 2016, A&A, 592, A11 (XXL Survey, XII)

Kuźmicz, A., & Jamrozy, M. 2012, MNRAS, 426, 851

Laing, R. A. 1988, Nature, 331, 149

Laing, R. A., Canvin, J. R., Bridle, A. H., & Hardcastle, M. J. 2006, MNRAS, 372, 510

Laing, R. A., Guidetti, D., Bridle, A. H., Parma, P., & Bondi, M. 2011, MNRAS, 417, 2789

Lara, L., Cotton, W. D., Feretti, L., et al. 2001a, A&A, 370, 409

Lara, L., Márquez, I., Cotton, W. D., et al. 2001b, A&A, 378, 826

Lavoie, S., Willis, J. P., Démoclès, J., et al. 2016, MNRAS, 462, 4141 (XXL Survey, XV)

Lieu, M., Smith, G. P., Giles, P. A., et al. 2016, A&A, 592, A4 (XXL Survey, IV)

Machalski, J., & Jamrozy, M. 2006, A&A, 454, 95

Machalski, J., Jamrozy, M., & Zola, S. 2001, A&A, 371, 445

Machalski, J., Koziel-Wierzbowska, D., & Jamrozy, M. 2007, Acta Astron., 57, 227

Malarecki, J. M., Jones, D. H., Saripalli, L., Staveley-Smith, L., & Subrahmanyan, R. 2015, MNRAS, 449, 955

McConnell, N. J., & Ma, C.-P. 2013, ApJ, 764, 184

McNamara, B. R., Nulsen, P. E. J., Wise, M. W., et al. 2005, Nature, 433, 45

Ochsenbein, F., Bauer, P., & Marcout, J. 2000, A&AS, 143, 23

Pacaud, F., Clerc, N., Giles, P. A., et al. 2016, A&A, 592, A2 (XXL Survey, II)

Pierre, M., Pacaud, F., Adami, C., et al. 2016, A&A, 592, A1 (XXL Survey, I)

Pompei, E., Adami, C., Eckert, D., et al. 2016, A&A, 592, A6 (XXL Survey, VII)

Proctor, D. D. 2016, ApJS, 224, 18

Ranalli, P., Comastri, A., & Setti, G. 2003, A&A, 399, 39

Raouf, M., Khosroshahi, H. G., Ponman, T. J., et al. 2014, MNRAS, 442, 1578

Rengelink, R. B., Tang, Y., de Bruyn, A. G., et al. 1997, A&AS, 124, 259

Robotham, A. S. G., Norberg, P., Driver, S. P., et al. 2011, MNRAS, 416, 2640

Sadler, E. M., Ekers, R. D., Mahony, E. K., Mauch, T., & Murphy, T. 2014, MNRAS, 438, 796

Safouris, V., Subrahmanyan, R., Bicknell, G. V., & Saripalli, L. 2009, MNRAS, 393, 2

Santiago-Bautista, I. d. C., Rodríguez-Rico, C. A., Andernach, H., et al. 2016, The Universe of Digital Sky Surveys, 42, 231

Saripalli, L., Gopal-Krishna, Reich, W., & Kuehr, H. 1986, A&A, 170, 20

Saripalli, L., Subrahmanyan, R., & Udaya Shankar N. 2002, ApJ, 565, 256

Saripalli, L., Hunstead, R. W., Subrahmanyan, R., & Boyce, E. 2005, AJ, 130, 896

Schoenmakers, A. P., de Bruyn, A. G., Röttgering, H. J. A., & van der Laan, H. 2001, A&A, 374, 861

Serra, A. L., & Diaferio, A. 2013, ApJ, 768, 116

Shimwell, T. W., Röttgering, H. J. A., Best, P. N., et al. 2017, A&A, 598, A104

Smolcic, V., Intema, H., Slaus, B., et al. 2018, A&A, 620, A14 (XXL Survey, XXIX)

Smolčić V. 2009, ApJ, 699, L43

Subrahmanyan, R., Saripalli, L., & Hunstead, R. W. 1996, MNRAS, 279, 257

Subrahmanyan, R., Saripalli, L., Safouris, V., & Hunstead, R. W. 2008, ApJ, 677, 63

Tasse, C., Cohen, A. S., Röttgering, H. J. A., et al. 2006, A&A, 456, 791

Tasse, C., Röttgering, H. J. A., Best, P. N., et al. 2007, A&A, 471, 1105

Tasse, C., Best, P. N., Röttgering, H., & Le Borgne D. 2008, A&A, 490, 893

Taylor, M. B. 2005, in Astronomical Data Analysis Software and Systems XIV, eds. P. Shopbell, M. Britton, & R. Ebert, Astronomical Society of the Pacific Conference Series, 347, 29

Taylor, A. R., Stil, J. M., & Sunstrum, C. 2009, ApJ, 702, 1230

Thorat, K., Saripalli, L., & Subrahmanyan, R. 2013, MNRAS, 434, 2877

Tumlinson, J., Peeples, M. S., & Werk, J. K. 2017, ARA&A, 55, 389

van Haarlem, M. P., Wise, M. W., Gunst, A. W., et al. 2013, A&A, 556, A2

Voit, G. M. 2005, Rev. Mod. Phys., 77, 207

Wardle, J. F. C., & Kronberg, P. P. 1974, ApJ, 194, 249

Wirth, A., Smarr, L., & Gallagher, J. S. 1982, AJ, 87, 602

Worrall, D. M., & Birkinshaw, M. 2006, in Physics of Active Galactic Nuclei at all Scales, ed. D. Alloin (Berlin: Springer Verlag), Lecture Notes in Physics, 693, 39

Worrall, D. M., Birkinshaw, M., & Cameron, R. A. 1995, ApJ, 449, 93

Wright, E. L., Eisenhardt, P. R. M., Mainzer, A. K., et al. 2010, AJ, 140, 1868

Appendix A: Mid-infrared photometry and optical spectra of the host galaxies

Table A.1 contains the WISE photometry and Table A.2 the optical and near-IR photometry. The optical spectra of the host galaxies are shown in Fig. A.1.

**Table A.1.** WISE photometry and colors of the host galaxies, taken from the cross-identification in SDSS DR14.

Source	W1	W2	W3	W1-W2	W2-W3
Exemplar	12.93	12.79	12.04	0.14	0.75
Double Irony	13.10	12.95	11.56	0.15	1.39
Difference	−0.17	−0.16	0.48	−0.01	−0.64

Notes. The galaxies are not detected in the W4 (22 μm) band. The detections are weak in the W3 (12 μm) band (signal-to-noise ratio, S/N, of 3.4 for the Exemplar, and S/N = 2.3 for the Double Irony) but the galaxies are clearly detected in the W1 (3.4 μm) and W2 (4.6 μm) bands. The WISE colors of the Exemplar and the Double Irony are consistent with those of FR I radio galaxies.

Table A.2. Optical and near-infrared photometry of the host galaxies.

Source	u	g	r	i	z	J	H	K_s
Exemplar	19.59 ± 0.08	17.43 ± 0.01	16.37 ± 0.00	15.90 ± 0.00	15.56 ± 0.01	15.5	14.742	14.176
Double Irony	19.26 ± 0.06	17.35 ± 0.91	16.26	15.82	15.47 ± 0.01	15.223	14.634	13.987
Mag. difference	0.33	0.08	0.11	0.08	0.09	0.28	0.11	0.189

Notes. The *ugriz* photometry is from the SDSS DR14 and the NIR photometry from 2MASS. The last line shows the magnitude difference between the Exemplar and the Double Irony.
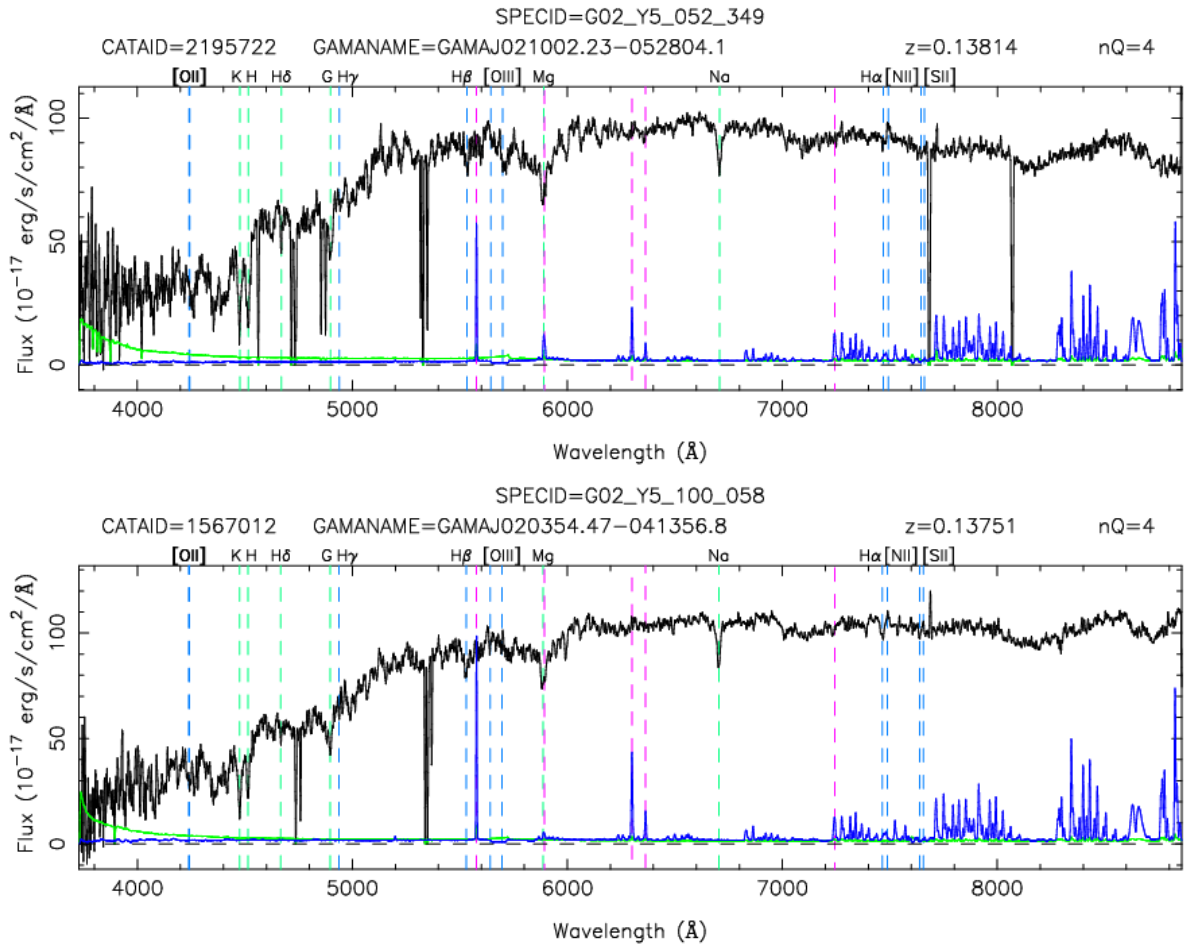
Fig. A.1. GAMA optical spectra of the host galaxies, displayed in the observer's frame. The green curve shows the noise level and the blue line is the sky spectrum. *Top panel:* the Exemplar. *Bottom panel:* the Double Irony. The two galaxies have remarkably similar optical spectra.